

The optimized point-coupling interaction for the relativistic energy density functional of Hartree-Bogoliubov approach quantifying the nuclear bulk properties

Zi Xin Liu^{a,b,c,*}, Yi Hua Lam^{a,b,*}, Ning Lu^{a,b,d} and Peter Ring^e

^a*Institute of Modern Physics, Chinese Academy of Sciences, Lanzhou 730000, People's Republic of China*

^b*School of Nuclear Science and Technology, University of Chinese Academy of Sciences, Beijing 100049, People's Republic of China*

^c*School of Physics Science and Technology, Lanzhou University, Lanzhou 730000, People's Republic of China*

^d*School of Nuclear Science and Technology, Lanzhou University, Lanzhou 730000, People's Republic of China*

^e*Fakultät für Physik, Technische Universität München, D-85748 Garching, Germany*

ARTICLE INFO

Keywords:

Nuclear Density Functional Theory
Relativistic Hartree-Bogoliubov
Point-coupling interactions
Binding energies and masses
Charge distribution
Saturation properties of nuclear matter

ABSTRACT

We propose a newly optimized nonlinear point-coupling parameterized interaction, PC-L3R, for the relativistic Hartree-Bogoliubov framework with a further optimized separable pairing force by fitting to observables, i.e., the binding energies of 91 spherical nuclei, charge radii of 63 nuclei, and 12 sets of mean pairing gaps consisting of 54 nuclei in total. The separable pairing force strengths of proton and neutron are optimized together with the point-coupling constants, and are justified in satisfactory reproducing the empirical pairing gaps. The comparison of experimental binding energies compiled in AME2020 for 91 nuclei with the ones generated from the present and other commonly used point-coupling interactions indicates that the implementation of PC-L3R in relativistic Hartree-Bogoliubov yields the lowest root-mean-square deviation. The charge radii satisfactory agree with experiment. Meanwhile, PC-L3R is capable of estimating the saturation properties of the symmetric nuclear matter and of appropriately predicting the isospin and mass dependence of binding energy. The experimental odd-even staggering of single nucleon separation energies is well reproduced. The comparison of the estimated binding energies for 7,373 nuclei based on the PC-L3R and other point-coupling interactions is also presented.

1. Introduction


With the recent advancements in radioactive ion beams and detectors, new experiments have revealed a wealth of structural phenomena in exotic nuclei with extreme isospin values, such as the halo phenomena [1], island of inversion [2], neutron skin [3], the disappearance of traditional magic numbers but with the occurrence of new ones [4, 5], masses and half lives of the neutron-rich nuclei important for understanding the synthesis of heavy elements in extreme astrophysical environments [6], and masses of proton-rich nuclei for Type-I X-ray bursts [7]. Hence, theoretical nuclear models capable of providing a satisfactory description of the ground-state properties and collective excitations of atomic nuclei, ranging from the relatively light to superheavy nuclei, from the spherical to deformed nuclei, and from the valley of β -stability to the particle-drip lines [8, 9, 10, 11, 12, 13, 14, 15, 16, 17, 18], are crucial for us to understand the interactions and configurations of nucleons in atomic nuclei.

The self-consistent relativistic mean-field (RMF) model with the Bardeen-Cooper-Schrieffer (BCS) method incorporating a nuclear density functional has been used to describe various nuclear properties [19] and to obtain the relevant nuclear physics input for astrophysical calculations [20, 21, 22]. Such calculations were based on the RMF+BCS frame-

work with the monopole pairing force, e.g., the δ pairing force [19, 23, 24, 25]. The BCS treatment on pairing force provides, however, a poor approximation for exotic nuclei far from the valley of β -stability [10]. The common understanding is that a consistent description of neutron-rich nuclei requires a unified and self-consistent treatment of mean-field and pairing correlations, which plays a critical role in exotic nuclei. Therefore, the self-consistent relativistic Hartree-Bogoliubov (RHB) framework was developed to unify the treatment of pairing correlations and mean-field potentials, and to analyze the structural phenomena in exotic nuclei [8, 26, 27, 28].

The most widely used effective interactions serving as the mean-field potential of the RMF and RHB frameworks are the meson-exchange [29, 30, 31, 32, 33, 34, 35]. In recent years, the point-coupling model offers an alternative to the meson-exchange model as the exchange of heavy mesons associated with short-distance dynamics cannot be resolved at low energies [19, 23, 36, 37, 38, 39, 40, 41, 42, 43, 44, 45]. The presently and commonly used point-coupling parameterized interactions include PC-PK1 [19], PC-F1 [23], PC-LA [36], and DD-PC1 [38]. The PC-LA parameterization does not consider a pairing force in the fitting procedure, whereas the PC-F1 and PC-PK1 interactions were fitted based on the RMF+BCS framework with the δ pairing force [19, 23, 24, 25]. The DD-PCX [40] and PC-X [41] interactions were recently proposed for the RHB model with a separable pairing force, however, its capability is yet to be assessed. Moreover, the proton and neutron pairing strengths

Corresponding authors:

liuzixin1908@impcas.ac.cn (Z.X. Liu); lamyihua@impcas.ac.cn (Y.H. Lam)
ORCID(s) 
0000-0001-5652-1516 (Z.X. Liu); 0000-0001-6646-0745 (Y.H. Lam);
0000-0002-3445-0451 (N. Lu); 0000-0001-7129-2942 (P. Ring)

in the separable pairing force of all presently available nonlinear point-coupling interactions are treated in an equal footing, and thus the separable pairing strength is not optimized. Hence, a robust and fully optimized point-coupling interaction accustomed to the RHB framework with justified pairing strengths is highly desired by the community to describe the experimentally determined finite nuclei and nuclear matter properties.

In this work, we propose a new set of fully optimized nonlinear point-coupling interaction for the RHB framework with a justified separable pairing force, named PC-L3R. We present the theoretical framework of the point-coupling interaction and relativistic Hartree-Bogoliubov model in Sec. 2. Then, we discuss the assessments of the new point-coupling interaction in Sec. 3, and show the comparison of the nuclear binding energies resulted from various point-coupling interactions in Sec. 4. Our summary is drawn in Sec 5.

2. Point-coupling interaction for the relativistic Hartree-Bogoliubov model

The effective covariant Lagrangian density of the point-coupling interaction for the relativistic mean field (RMF) model is expressed as [10, 11]

$$\mathcal{L} = \mathcal{L}^{\text{free}} + \mathcal{L}^{4f} + \mathcal{L}^{\text{ho}} + \mathcal{L}^{\delta} + \mathcal{L}^{\text{em}}, \quad (1)$$

where $\mathcal{L}^{\text{free}}$ is the free nucleons terms,

$$\mathcal{L}^{\text{free}} = \bar{\psi}(i\gamma_{\mu}\partial^{\mu} - M)\psi, \quad (2)$$

\mathcal{L}^{4f} is the four-fermion point-coupling terms,

$$\begin{aligned} \mathcal{L}^{4f} = & -\frac{1}{2}\alpha_S(\bar{\psi}\psi)(\bar{\psi}\psi) - \frac{1}{2}\alpha_V(\bar{\psi}\gamma_{\mu}\psi)(\bar{\psi}\gamma^{\mu}\psi) \\ & - \frac{1}{2}\alpha_{TV}(\bar{\psi}\vec{\tau}\gamma_{\mu}\psi) \cdot (\bar{\psi}\vec{\tau}\gamma^{\mu}\psi), \end{aligned} \quad (3)$$

\mathcal{L}^{ho} is the higher-order terms, which take into account of the effects of medium dependence,

$$\begin{aligned} \mathcal{L}^{\text{ho}} = & -\frac{1}{3}\beta_S(\bar{\psi}\psi)^3 - \frac{1}{4}\gamma_V[(\bar{\psi}\gamma_{\mu}\psi)(\bar{\psi}\gamma^{\mu}\psi)]^2 \\ & - \frac{1}{4}\gamma_S(\bar{\psi}\psi)^4, \end{aligned} \quad (4)$$

\mathcal{L}^{δ} is the gradient terms,

$$\begin{aligned} \mathcal{L}^{\delta} = & -\frac{1}{2}\delta_S\partial_{\nu}(\bar{\psi}\psi)\partial^{\nu}(\bar{\psi}\psi) - \frac{1}{2}\delta_V\partial_{\nu}(\bar{\psi}\gamma_{\mu}\psi)\partial^{\nu}(\bar{\psi}\gamma^{\mu}\psi) \\ & - \frac{1}{2}\delta_{TV}\partial_{\nu}(\bar{\psi}\vec{\tau}\gamma_{\mu}\psi)\partial^{\nu}(\bar{\psi}\vec{\tau}\gamma_{\mu}\psi), \end{aligned} \quad (5)$$

and \mathcal{L}^{em} is the electromagnetic interaction terms,

$$\mathcal{L}^{\text{em}} = -\frac{1}{4}F^{\mu\nu}F_{\mu\nu} - e\frac{(1-\tau_3)}{2}\bar{\psi}\gamma^{\mu}\psi A_{\mu}. \quad (6)$$

M in Eq. (2) is the nucleon mass. $\vec{\tau}$ in Eqs. (3) and (5) is the isospin vector of the third component, τ_3 . In Eqs. (3), (4), and (5), α_S , α_V , α_{TV} , β_S , γ_S , γ_V , δ_S , δ_V , δ_V , and δ_{TV} are the respective coupling constants. The rotational symmetry

of each coupling constant is indicated by the subscript. S and V refer to the scalar and vector nucleon fields, respectively. TV refers to the isovector fields. A_{μ} and $F_{\mu\nu}$ are the four-vector potential and field strength tensor of the electromagnetic field, respectively.

With implementing the effective Lagrangian density, the relativistic Hartree-Bogoliubov (RHB) model that unifies the self-consistent mean field and a pairing field had been developed to describe the properties of open-shell nuclei [8, 26, 27, 28]. Here, we use the point-coupling effective covariant Lagrangian density described above to be the self-consistent mean field of the RHB model, and take the separable form of the pairing force [40, 41, 46, 47, 48] to be the pairing field. The RHB energy density functional is given as

$$E_{\text{RHB}}[\rho, \kappa] = E_{\text{RMF}}[\rho] + E_{\text{pair}}[\kappa], \quad (7)$$

where E_{RMF} is the self-consistent mean field term, and the pairing term reads

$$E_{\text{pair}}[\kappa] = \frac{1}{4} \sum_{n_1 n'_1} \sum_{n_2 n'_2} \kappa_{n_1 n'_1}^* \langle n_1 n'_1 | V^{pp} | n_2 n'_2 \rangle \kappa_{n_2 n'_2}, \quad (8)$$

where n refers to the original basis, e.g., an oscillator basis, or the coordinates in space, spin and isospin (\mathbf{r}, s, t). The normal density, ρ , and the pairing tensor, κ are given as

$$\rho_{nn'} = \langle \Phi_0 | c_n^{\dagger} c_n | \Phi_0 \rangle, \text{ and } \kappa_{nn'} = \langle \Phi_0 | c_n c_n | \Phi_0 \rangle, \quad (9)$$

respectively. $|\Phi_0\rangle$ is the ground state for an even-even nucleus. c_n^{\dagger} and c_n are the single-nucleon creation and annihilation operators, respectively. In the unitary Bogoliubov transformation, the single-nucleon operators is defined as the quasiparticle operators [49],

$$\beta_k^{\dagger} = \sum_n U_{nk} c_n^{\dagger} + V_{nk} c_n, \quad (10)$$

and $|\Phi_0\rangle$ is represented as a vacuum with respect to quasiparticles

$$|\Phi_0\rangle = \prod_k \beta_k |0\rangle, \quad (11)$$

and $|0\rangle$ is the bare vacuum.

The RHB equation for nucleons is derived by the variational procedure,

$$\int d^3\mathbf{r}' \begin{pmatrix} h_D - \lambda_{\tau} & \Delta \\ -\Delta^* & -h_D^* + \lambda_{\tau} \end{pmatrix} \begin{pmatrix} U_k \\ V_k \end{pmatrix} = E_k \begin{pmatrix} U_k \\ V_k \end{pmatrix}, \quad (12)$$

where E_k is the quasiparticle energy, λ_{τ} ($\tau = n, p$) is chemical potential, U_k and V_k are quasiparticle wave functions and h_D is the Dirac Hamiltonian,

$$h_D(\mathbf{r}) = \boldsymbol{\alpha} \cdot \mathbf{p} + V(\mathbf{r}) + \beta(M + S(\mathbf{r})), \quad (13)$$

where $\boldsymbol{\alpha}$ and β are the Dirac matrices, p is the momentum operator, and the scalar and vector potentials are

$$S(\mathbf{r}) = \alpha_S \rho_S + \beta_S \rho_S^2 + \gamma_S \rho_S^3 + \delta_S \Delta \rho_S \text{ and}$$

The optimized point-coupling interaction for the relativistic energy density functional of Hartree-Bogoliubov approach

$$V(\mathbf{r}) = \alpha_V \rho_V + \gamma_V \rho_V^3 + \delta_V \Delta \rho_V + e A_0 \\ + \alpha_{TV} \tau_3 \rho_{TV} + \delta_{TV} \tau_3 \Delta \rho_{TV},$$

respectively. The local densities are

$$\rho_S(\mathbf{r}) = \sum_{k>0} \bar{V}_k(\mathbf{r}) V_k(\mathbf{r}), \\ \rho_V(\mathbf{r}) = \sum_{k>0} V_k^\dagger(\mathbf{r}) V_k(\mathbf{r}), \text{ and} \\ \rho_{TV}(\mathbf{r}) = \sum_{k>0} V_k^\dagger(\mathbf{r}) \tau_3 V_k(\mathbf{r}). \quad (14)$$

The pairing field Δ in Eq. (12) reads

$$\Delta_{n_1 n'_1} = \frac{1}{2} \sum_{n_2 n'_2} \langle n_1 n'_1 | V^{pp} | n_2 n'_2 \rangle \kappa_{n_2 n'_2}. \quad (15)$$

The pairing force that we use in Eq. (15) is the separable form of the pairing force, which is adjusted to model the pairing term of the finite range Gogny D1S force [50] in the particle-particle channel. The implementation of this separable form of the pairing force in the framework of RHB model produces the pairing properties of the nuclear matter and of finite nuclei in the same footing as the effect yielded from the corresponding pairing Gogny interaction [46]. The separable form of the pairing force is expressed as

$$V^{pp}(\mathbf{r}_1, \mathbf{r}_2, \mathbf{r}'_1, \mathbf{r}'_2) = -G \delta(\mathbf{R} - \mathbf{R}') P(\mathbf{r}) P(\mathbf{r}') \frac{1}{2} (1 - P^\sigma), \quad (16)$$

with the center of mass, $\mathbf{R} = (\mathbf{r}_1 + \mathbf{r}_2)/2$, and the relative coordinates, $\mathbf{r} = \mathbf{r}_1 - \mathbf{r}_2$. The form factor $P(\mathbf{r})$ is of Gaussian shape

$$P(\mathbf{r}) = \frac{1}{(4\pi a^2)^{3/2}} e^{-r^2/4a^2}. \quad (17)$$

According to Tian *et al.* [46], the G strength in Eq. (16) and the a parameter in Eq. (17) are defined as -728 MeV fm^3 and 0.644 fm , respectively. We can in fact follow the procedure of Yüksel *et al.* [40] to further optimize these G and a factors with separating the G strength to neutron (G_n) and proton (G_p) pairing strengths to improve the description of the bulk nuclear properties.

3. PC-L3R, the optimized coupling constants and pairing strengths for the RHB model

We perform a series of grid search up to $\approx 10^9$ calculations with cross validation for 91 spherical nuclei to obtain a set of optimized coupling constants, and the G_n , G_p , and a factors in the separable pairing force. The mean pairing gaps are calculated using the five-point formula [51]. The observables of 65 spherical nuclei selected in the previous work [19] were also included for fitting the present point coupling interaction. The configuration space of harmonic oscillator wave functions with appropriate symmetry is employed to

solve the RHB equation for nucleons. The densities are computed in the coordinate space. The fermionic shells, $N_f=26$, is adopted for these calculations.

Meanwhile, we use the χ^2 minimization to isolate and to confine the relativistic point-coupling and pairing-strength parameter space. The minimization is quantified as below,

$$\chi^2(\mathbf{P}) = \sum_{i=1}^{N_i} \sum_{j=1}^{n_i} \left(\frac{O_{i,j}^{\text{cal.}}(\mathbf{P}) - O_{i,j}^{\text{exp.}}}{\Delta O_i} \right)^2 \quad (18)$$

where \mathbf{P} is the parameter set, $\mathbf{P} = (P_1, P_2, \dots, P_n)$. N_i is a set of physical observables, e.g., binding energies, charge radii, and empirical pairing gaps. Each type of observable with the label i is associated with a set of n_i data points. For the theoretical weight, ΔO_i , we refer to the previous works [19, 38, 40, 41] and assess several ΔO_{BE} , see Fig. S1a. With studying several sets of the optimized theoretical weights, ΔO_i for binding energies, charge radii, and empirical pairing gaps, are defined as $\Delta O_{\text{BE}} = 1 \text{ MeV}$ (91 nuclei), $\Delta O_{\text{CR}} = 0.02 \text{ fm}$ (63 nuclei), and $\Delta O_{\text{PG}} = 0.1 \text{ MeV}$ (twelve sets of mean pairing gaps consisting of 54 nuclei in total), respectively. Note that the consideration of the influence on the single neutron separation energies further help confines the pairing strengths. This new set of point-coupling interaction is named PC-L3R (Table 1), which consists of the nine coupling constants in Eqs. (3), (4), and (5), the G_n and G_p pairing strengths and a factor in Eqs. (16) and (17). The test of naturalness for nine coupling constants of PC-L3R indicates that these coupling constants are natural (Supplemental Material (SM) and Table S2).

We then assess the influence of the PC-L3R interaction on the ground state properties, i.e., binding energies and available charge radii of these 91 finite nuclei and the saturation properties of symmetric nuclear matter as follows.

Binding energies of the selected spherical nuclei – The root mean square (rms) deviation values and the root of relative square (rrs) percentages of comparing the theoretical and experimental binding energies of 60, 65, and 91 spherical nuclei are listed in Table 2. The present optimized PC-L3R interaction used in the RHB model with the separable pairing force yields the lowest rms values, i.e., 1.176 MeV (rms₆₀), 1.245 MeV (rms₆₅), and 1.339 MeV (rms₉₁). The PC-PK1, or PC-X, or DD-PC1, or DD-PCX, or PC-F1, or PC-LA interaction in the RHB model with the separable pairing force produces a rather high rms deviations, 1.248–3.269 MeV (rms₆₀), 1.312–3.206 MeV (rms₆₅), and 1.453–2.925 MeV (rms₉₁) (models labeled with a superscript asterisk in Table 2). The experimental and theoretical binding energies of the selected 91 spherical nuclei are listed in Table S3. Hereafter, the labels of all models with the specific point-coupling interaction and pairing force are referred to the footnote of Table 2, except when otherwise specified.

Charge radii of the selected spherical nuclei – The theoretical radii of the selected 63 spherical nuclei are compared with the updated experimental data [53] (Table S4). Overall, the low rms deviations, 0.0153–0.0211 fm, of comparing the calculated radii from each theoretical model with

Table 1

The PC-L3R point-coupling constants, pairing strengths, and the respective uncertainties.

Coupling constant	Quantity, uncertainty ^a and physical unit(s)
α_S	$-3.99289 \pm 0.00004 \times 10^{-04} \text{ MeV}^{-2}$
β_S	$8.65504 \pm 0.0007 \times 10^{-11} \text{ MeV}^{-5}$
γ_S	$-3.83950 \pm 0.0009 \times 10^{-17} \text{ MeV}^{-8}$
δ_S	$-1.20749 \pm 0.0055 \times 10^{-10} \text{ MeV}^{-4}$
α_V	$2.71991 \pm 0.00004 \times 10^{-04} \text{ MeV}^{-2}$
γ_V	$-3.72107 \pm 0.008 \times 10^{-18} \text{ MeV}^{-8}$
δ_V	$-4.26653 \pm 0.005 \times 10^{-10} \text{ MeV}^{-4}$
α_{TV}	$2.96688 \pm 0.016 \times 10^{-05} \text{ MeV}^{-2}$
δ_{TV}	$-4.65682 \pm 0.25 \times 10^{-10} \text{ MeV}^{-4}$
G_n	$-749.552 \pm 3.5 \text{ MeV fm}^3$
G_p	$-680.080 \pm 20 \text{ MeV fm}^3$
a	$0.62948 \pm 0.0015 \text{ fm}$

NOTE

^a The uncertainties of the coupling constants and pairing strengths are constrained by the close reproduction of the root-mean-square deviation (rms) value, 1.339 MeV (Table 2), of comparing the theoretical and experimental binding energies of 91 spherical nuclei listed in Table S3. The close reproduction of rms is limited to $\lesssim 20$ keV different from the rms. Meanwhile, the rms of the charge radii of 63 nuclei is maintained in the range of $0.0185 \leq \text{rms} \leq 0.0187$, and the change of χ^2 in Eq.(18) is limited to $\Delta\chi^2(\mathbf{P}) \lesssim 5$.

experimental radii indicate that all theoretical radii are in good agreement with experiment, especially the DD-PCX and PC-F1 yields the lowest rms deviation, 0.0153 fm. The rms value of the RHB model with PC-L3R interaction, 0.0224 fm (rms_{23}) and 0.0187 fm (rms_{63}), closely aligns with the rms values of other theoretical models (Table 2). In additions, the neutron skin thickness of ^{208}Pb produced from PC-L3R is closely aligned with the results of RHB frameworks using other nonlinear point-coupling interactions, and agrees with the latest PREX-2 experiment [54] (Fig. S2).

Saturation properties of the symmetric nuclear matter

– These properties include the saturation density, ρ_0 , binding energy per nucleon, E/A , effective Dirac mass, M^* , incompressibility, K_0 , symmetry energy, E_{sym} , and slope of symmetry energy, L_0 .

Comparing the properties generated by PC-L3R with the ones resulted from PC-PK1 [19], PC-X [41], DD-PC1 [38], DD-PCX [40], PC-F1 [23], and PC-LA [36], we find that all point-coupling interactions produce a set of rather similar ρ_0 with the average as $0.152_{-0.004}^{+0.002} \text{ fm}^{-3}$, and E/A with the average as $-16.11_{-0.06}^{+0.08} \text{ MeV}$ (Table 3). This indicates that PC-L3R not only exhibits the capability of describing the saturation properties of nuclear matter conformed with other nonlinear effective point-coupling interactions, but also agrees with the empirical $\rho_0 = 0.166 \pm 0.018 \text{ fm}^{-3}$ and $E/A = -16 \pm 1 \text{ MeV}$ [55]. Besides, we note that the nonlinear effective interactions PC-L3R, PC-PK1, PC-F1, PC-LA, and PC-X produce a set of ρ_0 and E/A values somehow larger than the saturation properties produced by the density dependence

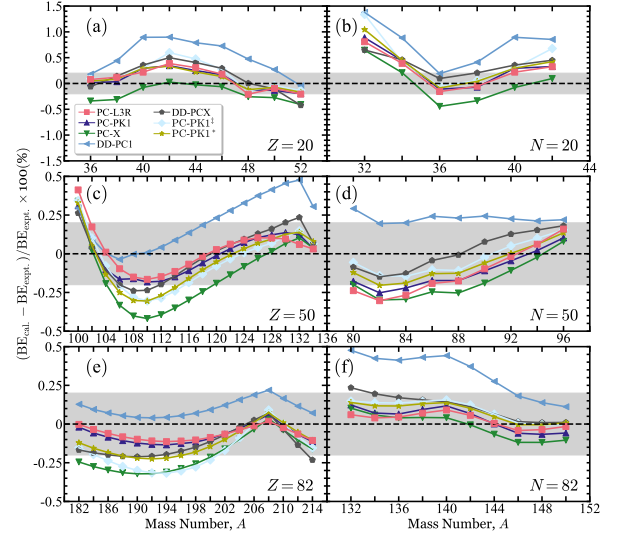


Figure 1: The relative accuracy of the theoretical description of the AME2020 experimental data [56] for the binding energies of the $Z=20, 50,$ and 82 isotopes, and for the $N=20, 50,$ and 82 isotones. See the footnote of Tables 2 and S3 for the theoretical frameworks in this figure. The gray regions in all panels are the $\pm 0.2\%$ error band.

point-coupling interactions, DD-PC1 and DD-PCX (Fig. S3).

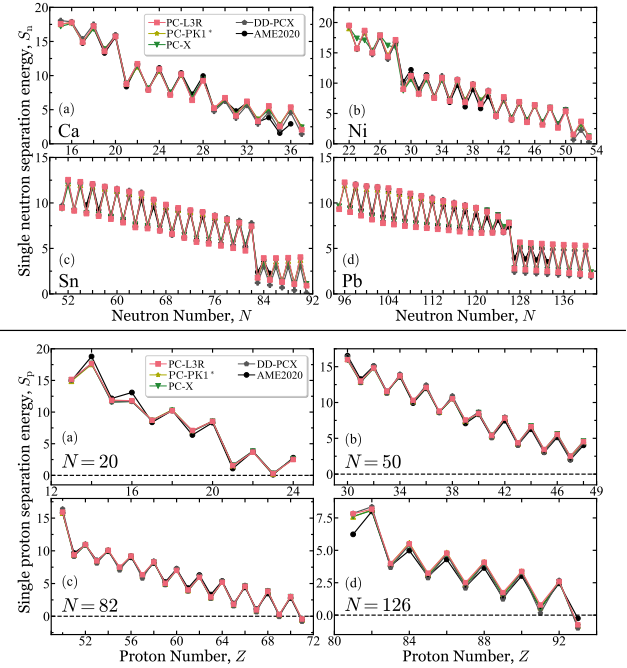


Figure 2: Single nucleon separation energy, S_i ($i=n$ or p), obtained from the AME2020 experimental data [56] (black dots) and from theoretical calculations. Top panel: S_n for the Ca, Ni, Sn, and Pb isotopes. Bottom panel: S_p for the $N=20, 50, 82,$ and 126 isotones. Experimental uncertainties are smaller than the symbol.

4. Binding energies of nuclei

Binding energies of isotopic and isotonic chains – We present the comparison of the experimental and theoretical binding energies for some isotopic and isotonic chains based on the point-coupling interactions PC-L3R, PC-PK1, PC-X, DD-PC1, and DD-PCX used in the RHB, RMF, and RCHB

Table 2

The root mean square (rms) deviation values and the root of relative square (rrs) percentages of comparing the theoretical and experimental binding energies (BE), and charge radii (CR) for 60, 65, and 91 spherical nuclei, using the PC-L3R, PC-PK1, PC-X, DD-PC1, DD-PCX, PC-F1, and PC-LA interactions. The numbers of the nuclei considered in the calculations are given in subscript. The detailed data is listed in Tables S3 and S4 in the Supplemental Material.

	PC-L3R ^a	PC-PK1 ^b	PC-PK1 ^{*c}	PC-PK1 ^{‡d}	PC-X ^e	DD-PC1 ^f	DD-PC1 ^{*g}	DD-PCX ^h	PC-F1 ⁱ	PC-F1 ^{*j}	PC-LA ^k	PC-LA ^{*l}	
BE	rms₆₀^m (MeV)	1.176	1.248	1.417	1.64	1.378	3.139	3.269	1.413	2.589	2.913	2.581	2.890
	rms₆₅ⁿ (MeV)	1.245	1.312	1.495	1.69	1.542	3.088	3.206	1.461	2.590	2.895	2.615	2.915
	rms₉₁^p (MeV)	1.339	1.453	1.796	2.11	2.168	2.805	2.925	1.712	2.493	2.755	2.555	2.714
	rrs₆₀ (%)	0.22%	0.18%	0.22%	0.39%	0.20%	0.47%	0.50%	0.22%	0.30%	0.39%	0.29%	0.34%
	rrs₆₅ (%)	0.23%	0.19%	0.23%	0.39%	0.22%	0.45%	0.49%	0.23%	0.32%	0.40%	0.30%	0.35%
rrs₉₁ (%)	0.24%	0.23%	0.27%	0.39%	0.27%	0.44%	0.48%	0.26%	0.35%	0.40%	0.32%	0.35%	
CR	rms₂₃^q (fm)	0.0224	0.0222	0.0220	0.0217	0.0222	0.0197	0.0197	0.0195	0.0197	0.0194	0.0250	0.0247
	rms₆₃^r (fm)	0.0187		0.0183	0.0182	0.0187		0.0157	0.0153		0.0153		0.0211
	rrs₂₃ (%)	0.68%	0.68%	0.67%	0.67%	0.69%	0.58%	0.59%	0.61%	0.61%	0.61%	0.67%	0.66%
	rrs₆₃ (%)	0.51%		0.50%	0.50%	0.52%		0.44%	0.43%		0.43%		0.51%

^a PC-L3R: calculated from the RHB model with the PC-L3R interaction. ^b PC-PK1: quoted from the RMF model with the Bardeen–Cooper–Schrieffer (BCS) theory using the PC-PK1 interaction [19] and δ pairing force. ^c PC-PK1^{*}: calculated from the RHB model using the PC-PK1 interaction [19] and separable pairing force [46]. ^d PC-PK1[‡]: quoted from the relativistic continuum Hartree-Bogoliubov (RCHB) model [52] using the PC-PK1 interaction [19] and δ pairing force. ^e PC-X: calculated from the RHB model using the PC-X interaction [41] and separable pairing force [46]. ^f DD-PC1: quoted from the RMF model with the BCS theory using the DD-PC1 interaction [38] and δ pairing force. ^g DD-PC1^{*}: calculated from the RHB model using the DD-PC1 interaction [38] and separable pairing force [46]. ^h DD-PCX: calculated from the RHB model using the DD-PCX interaction [40] and separable pairing force [40]. ⁱ PC-F1: quoted from the RMF model with the BCS theory using the PC-F1 interaction [23] and δ pairing force. ^j PC-F1^{*}: calculated from the RHB model using the PC-F1 interaction [23] and separable pairing force [46]. ^k PC-LA: quoted from the RMF model with the BCS theory using the PC-LA interaction [36] and δ pairing force. ^l PC-LA^{*}: calculated from the RHB model using the PC-LA interaction [36] and separable pairing force [46]. The rms values and rrs percentages are expressed as, $\text{rms}_i = \left[\left(\sum_j^N |E_j^{\text{expt}} - E_j^{\text{calc}}|^2 \right) / N \right]^{1/2}$ and $\text{rrs}_i = \left[\left(\sum_j^N |E_j^{\text{expt}} - E_j^{\text{calc}}|^2 / (E_j^{\text{expt}})^2 \right) / N \right]^{1/2}$, respectively. ^m rms₆₀ (bold text): obtained from comparing the experimental and theoretical binding energies of 60 spherical nuclei, selected for fitting the PC-PK1 [19]. ⁿ rms₆₅ (blue text): obtained from comparing the experimental and theoretical binding energies of 65 spherical nuclei, referred by previous works in fitting point coupling interactions [19, 40, 41]. ^o rms₉₁: obtained from comparing the experimental and theoretical binding energies of 91 spherical nuclei, selected for fitting the PC-L3R. ^p rms₂₃ (bold text): obtained from comparing the experimental and theoretical charge radii of 23 spherical nuclei, selected for fitting the PC-PK1 [19]. ^r rms₆₃: obtained from comparing the experimental and theoretical charge radii of 63 spherical nuclei, selected for fitting the PC-L3R. The rrs have a similar label as rms.

Table 3

The saturation properties of nuclear matter estimated by the non-linear point-coupling interactions, i.e., PC-L3R, PC-PK1 [19], PC-X [41], PC-F1 [23], and PC-LA [36] and the density-dependent point-coupling interactions, DD-PC1 [38] and DD-PCX [40]. The symmetric nuclear matter energy plot is shown in Fig. S3.

	PC-L3R	PC-PK1	PC-X	DD-PC1	DD-PCX	PC-F1	PC-LA
ρ_0 (fm ⁻³)	0.153	0.154	0.154	0.152	0.152	0.151	0.148
E/A (MeV)	-16.12	-16.12	-16.14	-16.06	-16.03	-16.17	-16.13
M^*/M	0.59	0.59	0.58	0.58	0.56	0.61	0.58
K_0 (MeV)	245	238	240	230	213	255	264
E_{sym} (MeV)	35.8	35.6	35.2	33	31	37.8	37.2
L_0 (MeV)	114	113	112	70	46	117	108

frameworks in Fig. 1. For the $Z=20$ (Ca) isotopes, $N=20$ and $N=50$ isotones, the results from PC-L3R, PC-PK1, and PC-PK1^{*} are rather similar, whereas for the $Z=50$ (Sn) and $Z=82$ (Pb) isotopes, especially for the even-even ^{122–134}Sn, the PC-PK1^{*} produces a set of binding energies more deviated from experiment compared to PC-L3R and PC-PK1, indicating the robustness of PC-L3R accustomed to the RHB model that yields an overall agreement with the prediction of PC-PK1 used in the RMF+BCS framework. We remark that a steep change at ²⁰⁸Pb is produced by PC-PK1, PC-PK1^{*}, PC-PK1[‡], PC-X, DD-PC1, and DD-PCX, whereas PC-L3R results a much more reduced dip change (lower left panel in Fig. 1). A similar characteristic also happens in the $Z=50$ isotopic chain at ¹³²Sn. For the $N=82$ isotones, PC-L3R reproduces the experimental binding energies with the average absolute deviation 0.535 MeV, whereas PC-PK1, PC-PK1^{*}, PC-PK1[‡], PC-X, DD-PC1, and DD-PCX produce the average absolute deviation of 0.839 MeV, 0.931 MeV, 1.07 MeV, 0.818 MeV, 4.278 MeV, and 1.274 MeV, respectively. This implies that the PC-L3R interaction is able to balance the Coulomb field and the isovector channel of the effective La-

grangian. Thus, PC-L3R provides an appropriate prediction for not only the binding energy but also the isospin dependence.

We then evaluate the contribution of pairing energy, the experimental and theoretical single neutron and proton separation energies for some isotopic and isotonic chains based on the RHB frameworks using point-coupling interactions PC-L3R, PC-PK1, PC-X, and DD-PCX listed in Table 2. For the present calculations of odd- N and/or odd- Z nuclei, we consider the blocking effects of the unpaired nucleon(s)¹. The PC-L3R adequately reproduces the experimental odd-even staggering trend of single nucleon separation energies (Fig. 2). The experimental single proton drip line at ¹⁵²Yb ($N=82$) and ²¹⁸U ($N=126$) are well reproduced by the RHB frameworks using point-coupling interactions PC-L3R, PC-PK1, and PC-X (subfigures (c) and (d) in the bottom panel of Fig. 2); nevertheless, the single proton drip line at ¹⁵²Yb ($N=82$) generated from DD-PCX is not consistent with the experimental data. Meanwhile, we find that the (absolute) magnitude of G_p is smaller than the G_n strength (Table 1). This is mainly due to the repulsive Coulomb force inducing a reduced pairing interaction for the protons [57].

β -decay $Q(Q_{\beta^-})$ values – Recent rapid-neutron capture (r -) process astrophysical models point out the decisive importance of β -decay half-lives of nuclei around magic neutron numbers $N=50$ and 82 [58]. We find that PC-L3R produces the lowest rms values for the Q_{β^-} values based on

¹The ground state of a nucleus with an odd neutron and/or proton number is one-quasiparticle state, $|\Phi_1\rangle = \beta_{\text{h}}^{\dagger} |\Phi_0\rangle$, which is constructed based on the ground state of an even-even nucleus $|\Phi_0\rangle$, c.f. Eq. (11), where β^{\dagger} is the single-nucleon creation operator and h denotes the blocked quasiparticle state occupied by the unpaired nucleon(s). See Ref. [49] for the detail description of using the blocking effect. The same technique is employed for calculating the mirror displacement energies along the $N=Z$ line [7].

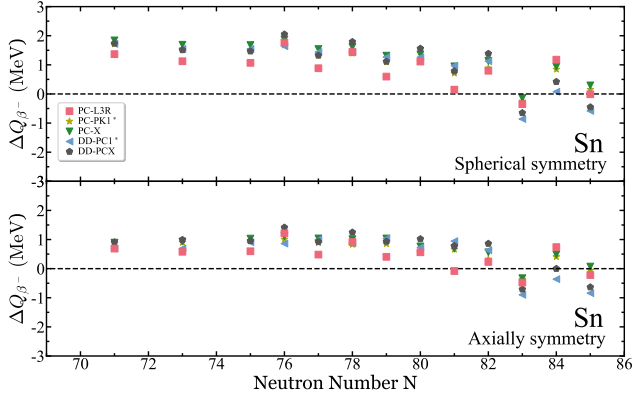


Figure 3: The deviations of the calculated Q_{β^-} values from the AME2020 experimental data for the Sn isotopic chain. The top (bottom) panel shows the results of spherical (axial) symmetry.

spherical- or axial-symmetry calculations, i.e., 1.038 MeV and 0.624 MeV, respectively. The further improvement imposed from the axial-symmetry calculation is due to the existence of shape variation in the Sb isotopic chain. The deviations of the Q_{β^-} values produced from the PC-L3R decreases with the increase of neutron number for the Sn isotopic chain (Fig. 3). This trend is very encouraging for us to use the PC-L3R interaction to predict the regions without experimentally determined Q_{β^-} values.

Binding energies of 7,373 nuclei – We also compute the binding energies of 7,373 nuclei using the RHB model with the PC-L3R interaction with an optimized separable pairing force. The comparison of both binding energies from PC-L3R and PC-PK1 † (PC-X) is given in Fig. 4a (4b). For the light to medium nuclei at the region $Z=8-50$ and $N=20-126$, the PC-L3R results are considerable close to the ones of PC-PK1 † and PC-X. We compare the theoretical energies with currently available experimental data [56] at the region $Z=65-90$ and $N=75-150$, encircled with the black line in Figs. 4a and 4b. The rrs for PC-L3R, PC-PK1 † , and PC-X is 0.586%, 0.69%, and 0.723%, respectively. Besides, the rrs produced from the DD-PC1 and DD-PCX are 0.518% and 0.692%, respectively.

For the heavy nuclei far from stability at regions $Z=60-110$ and $N=126-184$, PC-PK1 † (PC-X) estimates a set of binding energies, up to 4.59 MeV (8.133 MeV) larger than the energies produced from PC-L3R. Meanwhile, for the region at $Z>82$ and $N>184$, the binding energies produced from PC-PK1 † and PC-X further deviate from the ones generated by PC-L3R; for PC-PK1 † and PC-X, the largest absolute deviation is 5.95 MeV and 7.500 MeV, respectively. We anticipate that the RHB with axial symmetry or triaxial deformation could further reduce the deviation between the theoretical and experiment binding energies for the region $Z=65-90$ and $N=75-150$.

5. Summary

In this work, we propose a newly optimized nonlinear point-coupling parameterized interaction, PC-L3R, for the RHB framework with a further optimized separable pair-

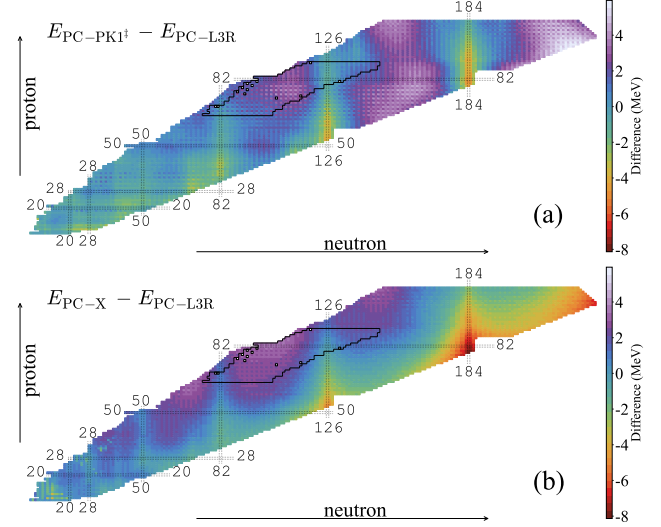


Figure 4: The comparison of the binding energies of 7,373 nuclei calculated from the PC-L3R with the ones produced by the PC-PK1 † (panel a) or PC-X (panel b). See the footnote of Table S3 for the theoretical frameworks of PC-PK1 † , PC-X, and PC-L3R. The blank squared nuclei are excluded in the present comparison due to either unknown or ambiguous experimental data.

ing force of G_n and G_p strengths (Table 1), which significantly improves the point-coupling interaction in describing the finite nuclear properties. The PC-L3R interaction is fitted to the observables of 91 spherical nuclei, i.e., the binding energies, charge radii, and another important constraint from pairing gaps. The lowest rms deviations, 1.176 MeV (rms_{60}), 1.245 MeV (rms_{65}), and 1.339 MeV (rms_{91}), yielded by the implementation of the PC-L3R interaction in the RHB framework with the separable pairing force indicates the robustness of PC-L3R in the RHB framework unifying the treatment of pairing correlations and mean-field potentials, compared to other point-coupling interactions, i.e., PC-PK1, PC-X, DD-PC1, DD-PCX, PC-F1, and PC-LA, which are either used in the RHB framework with the separable pairing force or the RMF+BCS framework with the δ pairing force, or PC-PK1 used in the RCHB framework with the δ pairing force (Table S3). Meanwhile, the PC-L3R for the RHB framework provides the same description as other point-coupling interactions for the charge radii of the selected 63 spherical nuclei, and produces a set of charge radii in a good agreement with experiment. A set of similar saturation properties is also obtained for the symmetric nuclear matter using the PC-L3R interaction, compared to the saturation properties generated from other point-coupling interactions.

We compare the experimental binding energies of the $Z=20, 50, 82$ isotopic and $N=20, 50, 82$ isotonic chains with the theoretical values resulted from the point-coupling interactions, PC-L3R, PC-PK1, PC-X, DD-PC1, and DD-PCX used in RHB, RMF+BCS, and RCHB frameworks. The PC-L3R provides an appropriate prediction for not only the binding energy but also for the isospin dependence. The PC-L3R has the potential to predict a set of theoretical Q_{β^-} values close to the future experimental Q_{β^-} at the $Z \geq 50, N > 82$ regions. The binding energies of 7,373

nuclei computed from the RHB model with the PC-L3R interaction are compared with the results from the RHB model with the PC-X interaction and with the ones from RCHB model with the PC-PK1 interaction [52]. The binding energies produced from PC-L3R, PC-PK1[‡], and PC-X are rather close at the relatively light region. For the heavy region at $Z=65-90$ and $N=75-150$, the PC-L3R provides the lowest rms deviation, 0.586%, among PC-L3R, PC-PK1[‡], and PC-X, compared with the currently available 807 experimental nuclear masses. The PC-L3R interaction could be a competently alternative point-coupling interaction for the RHB framework.

Declaration of competing interest

The authors declare that they have no known competing financial interests or personal relationships that could have appeared to influence the work reported in this paper.

Acknowledgments

This work was financially supported by the Strategic Priority Research Program of Chinese Academy of Sciences (CAS, Grant Nos. XDB34020100) and National Natural Science Foundation of China (No. 11775277). We are appreciative of the computing resource provided by the Institute of Physics (PHYS_T3 cluster) and Academia Sinica Grid Computing Center (Grant No. AS-CFII-112-103; QDR4 and FDR5 clusters) of Academia Sinica, Taiwan. Part of the numerical calculations were performed at the Gansu Advanced Computing Center. YHL gratefully acknowledges the financial supports from the Chinese Academy of Sciences President's International Fellowship Initiative (No. 2019FYM0002) and appreciates the laptop (Dell M4800) partially sponsored by Pin-Kok Lam and Fong-Har Tang during the pandemic of COVID-19. PR gratefully acknowledges financial support from the Deutsche Forschungsgemeinschaft (DFG, German Research Foundation) under Germany Excellence Strategy EXC-2094-390783311.

A. Supplementary material

Supplementary material related to this article is attached in this preprint.

CRedit authorship contribution statement

Zi Xin Liu: Conceptualization of this study, Fitting PC-L3R, Writing - Original draft preparation. **Yi Hua Lam:** Conceptualization of this study, Fitting PC-L3R, Writing - Original draft preparation. **Ning Lu:** Writing - Original draft preparation. **Peter Ring:** Important suggestions, Writing - Original draft preparation.

References

[1] I. Tanihata, H. Savajols, R. Kanungo, Prog. Part. Nucl. Phys. 68 (2013) 215. URL: <https://www.sciencedirect.com/science/article/pii/S0146641012001081>. doi:10.1016/j.pnnp.2012.07.001.

[2] F. Nowacki, A. Obertelli, A. Poves, Prog. Part. Nucl. Phys. 120 (2021) 103866. URL: <https://www.sciencedirect.com/science/article/pii/S014664102100020X>. doi:10.1016/j.pnnp.2021.103866.

[3] H. Sakaguchi, J. Zenihiro, Prog. Part. Nucl. Phys. 97 (2017) 1. URL: <https://www.sciencedirect.com/science/article/pii/S0146641017300546>. doi:10.1016/j.pnnp.2017.06.001.

[4] A. Ozawa, T. Kobayashi, T. Suzuki, K. Yoshida, I. Tanihata, Phys. Rev. Lett. 84 (2000) 5493. URL: <https://link.aps.org/doi/10.1103/PhysRevLett.84.5493>. doi:10.1103/PhysRevLett.84.5493.

[5] F. Wienholtz, D. Beck, K. Blaum, C. Borgmann, M. Breitenfeldt, R. B. Cakirli, S. George, F. Herfurth, J. D. Holt, M. Kowalka, S. Kreim, D. Lunney, V. Manea, J. Menéndez, D. Neidherr, M. Rosenbusch, L. Schweikhard, A. Schwenk, J. Simonis, J. Stanja, R. N. Wolf, K. Zuber, Nature 498 (2013) 346. URL: <https://www.nature.com/articles/nature12226>. doi:10.1038/nature12226.

[6] T. Marketin, L. Huther, G. Martínez-Pinedo, Phys. Rev. C 93 (2016) 025805. URL: <https://link.aps.org/doi/10.1103/PhysRevC.93.025805>. doi:10.1103/PhysRevC.93.025805.

[7] Y. H. Lam, Z. X. Liu, A. Heger, N. Lu, A. M. Jacobs, Z. Johnston, Astrophys. J. 929 (2022) 72. URL: <https://doi.org/10.3847/1538-4357/ac4d8b>. doi:10.3847/1538-4357/ac4d8b.

[8] P. Ring, Prog. Part. Nucl. Phys. 37 (1996) 193. URL: <https://www.sciencedirect.com/science/article/pii/0146641096000543>. doi:10.1016/0146-6410(96)00054-3.

[9] M. Bender, P.-H. Heenen, P.-G. Reinhard, Rev. Mod. Phys. 75 (2003) 121. URL: <https://link.aps.org/doi/10.1103/RevModPhys.75.121>. doi:10.1103/RevModPhys.75.121.

[10] D. Vretenar, A. V. Afanasjev, G. A. Lalazissis, P. Ring, Phys. Rep. 409 (2005) 101. URL: <https://www.sciencedirect.com/science/article/pii/S0370157304004545>. doi:10.1016/j.physrep.2004.10.001.

[11] J. Meng, H. Toki, S.-G. Zhou, S. Q. Zhang, W. H. Long, L. S. Geng, Prog. Part. Nucl. Phys. 57 (2006) 470. URL: <https://www.sciencedirect.com/science/article/pii/S014664100500075X>. doi:10.1016/j.pnnp.2005.06.001.

[12] S. Goriely, S. Hilaire, M. Girod, S. Péru, Phys. Rev. Lett. 102 (2009) 242501. URL: <https://link.aps.org/doi/10.1103/PhysRevLett.102.242501>. doi:10.1103/PhysRevLett.102.242501.

[13] M. Kortelainen, T. Lesinski, J. Moré, V. Nazarewicz, J. Sarich, N. Schunck, M. V. Stoitsov, S. Wild, Phys. Rev. C 82 (2010) 024313. URL: <https://link.aps.org/doi/10.1103/PhysRevC.82.024313>. doi:10.1103/PhysRevC.82.024313.

[14] T. Nikšić, D. Vretenar, P. Ring, Prog. Part. Nucl. Phys. 66 (2011) 519. URL: <https://www.sciencedirect.com/science/article/pii/S0146641011000561>. doi:10.1016/j.pnnp.2011.01.055.

[15] J. Meng, S.-G. Zhou, J. Phys. G: Nucl. Part. Phys. 42 (2015) 093101. URL: <https://doi.org/10.1088/0954-3899/42/9/093101>. doi:10.1088/0954-3899/42/9/093101.

[16] A. Afanasjev, S. Agbemava, A. Gyawali, Phys. Lett. B 782 (2018) 533–540. URL: <https://www.sciencedirect.com/science/article/pii/S0370269318304349>. doi:https://doi.org/10.1016/j.physletb.2018.05.070.

[17] T.-T. Sun, Z.-X. Liu, L. Qian, B. Wang, W. Zhang, Phys. Rev. C 99 (2019) 054316. URL: <https://link.aps.org/doi/10.1103/PhysRevC.99.054316>. doi:10.1103/PhysRevC.99.054316.

[18] S. E. Agbemava, A. V. Afanasjev, A. Taninah, A. Gyawali, Phys. Rev. C 99 (2019) 034316. URL: <https://link.aps.org/doi/10.1103/PhysRevC.99.034316>. doi:10.1103/PhysRevC.99.034316.

[19] P. W. Zhao, Z. P. Li, J. M. Yao, J. Meng, Phys. Rev. C 82 (2010) 054319. URL: <https://link.aps.org/doi/10.1103/PhysRevC.82.054319>. doi:10.1103/PhysRevC.82.054319.

[20] B. Sun, F. Montes, L. S. Geng, H. Geissel, Y. A. Litvinov, J. Meng, Phys. Rev. C 78 (2008) 025806. URL: <https://link.aps.org/doi/10.1103/PhysRevC.78.025806>. doi:10.1103/PhysRevC.78.025806.

[21] Z. M. Niu, B. Sun, J. Meng, Phys. Rev. C 80 (2009) 065806. URL: <https://link.aps.org/doi/10.1103/PhysRevC.80.065806>. doi:10.1103/PhysRevC.80.065806.

[22] X. D. Xu, B. Sun, Z. M. Niu, Z. Li, Y.-Z. Qian, J. Meng, Phys. Rev. C 87 (2013) 015805. URL: <https://link.aps.org/doi/10.1103/PhysRevC.87.015805>. doi:10.1103/PhysRevC.87.015805.

- PhysRevC.87.015805. doi:10.1103/PhysRevC.87.015805.
- [23] T. Bürvenich, D. G. Madland, J. A. Maruhn, P.-G. Reinhard, Phys. Rev. C 65 (2002) 044308. URL: <https://link.aps.org/doi/10.1103/PhysRevC.65.044308>. doi:10.1103/PhysRevC.65.044308.
- [24] T. Nikšić, D. Vretenar, P. Ring, Phys. Rev. C 73 (2006) 034308. URL: <https://link.aps.org/doi/10.1103/PhysRevC.73.034308>. doi:10.1103/PhysRevC.73.034308.
- [25] T. Nikšić, D. Vretenar, P. Ring, Phys. Rev. C 74 (2006) 064309. URL: <https://link.aps.org/doi/10.1103/PhysRevC.74.064309>. doi:10.1103/PhysRevC.74.064309.
- [26] H. Kucharek, P. Ring, Z. Phys. A 339 (1991) 23. URL: <https://link.springer.com/article/10.1007/BF01282930>. doi:10.1007/BF01282930.
- [27] J. Meng, P. Ring, Phys. Rev. Lett. 77 (1996) 3963. URL: <https://link.aps.org/doi/10.1103/PhysRevLett.77.3963>. doi:10.1103/PhysRevLett.77.3963.
- [28] W. Pöschl, D. Vretenar, G. A. Lalazissis, P. Ring, Phys. Rev. Lett. 79 (1997) 3841. URL: <https://link.aps.org/doi/10.1103/PhysRevLett.79.3841>. doi:10.1103/PhysRevLett.79.3841.
- [29] G. A. Lalazissis, J. König, P. Ring, Phys. Rev. C 55 (1997) 540. URL: <https://link.aps.org/doi/10.1103/PhysRevC.55.540>. doi:10.1103/PhysRevC.55.540.
- [30] S. Typel, H. H. Wolter, Nucl. Phys. A 656 (1999) 331. URL: <https://www.sciencedirect.com/science/article/pii/S0375947499003103>. doi:10.1016/S0375-9474(99)00310-3.
- [31] T. Nikšić, D. Vretenar, P. Finelli, P. Ring, Phys. Rev. C 66 (2002) 024306. URL: <https://link.aps.org/doi/10.1103/PhysRevC.66.024306>. doi:10.1103/PhysRevC.66.024306.
- [32] H. Abusara, A. V. Afanasjev, P. Ring, Phys. Rev. C 85 (2012) 024314. URL: <https://link.aps.org/doi/10.1103/PhysRevC.85.024314>. doi:10.1103/PhysRevC.85.024314.
- [33] M. Dutra, O. Lourenço, S. S. Avancini, B. V. Carlson, A. Delfino, D. P. Menezes, C. Providência, S. Typel, J. R. Stone, Phys. Rev. C 90 (2014) 055203. URL: <https://link.aps.org/doi/10.1103/PhysRevC.90.055203>. doi:10.1103/PhysRevC.90.055203.
- [34] W.-L. Lu, Z.-X. Liu, S.-H. Ren, W. Zhang, T.-T. Sun, J. Phys. G: Nucl. Part. Phys. 44 (2017) 125104. URL: <https://doi.org/10.1088/1361-6471/aa8e2d>. doi:10.1088/1361-6471/aa8e2d.
- [35] Z.-X. Liu, C.-J. Xia, W.-L. Lu, Y.-X. Li, J. N. Hu, T.-T. Sun, Phys. Rev. C 98 (2018) 024316. URL: <https://link.aps.org/doi/10.1103/PhysRevC.98.024316>. doi:10.1103/PhysRevC.98.024316.
- [36] B. A. Nikolaus, T. Hoch, D. G. Madland, Phys. Rev. C 46 (1992) 1757. URL: <https://link.aps.org/doi/10.1103/PhysRevC.46.1757>. doi:10.1103/PhysRevC.46.1757.
- [37] J. J. Ruskak, R. J. Furnstahl, Nucl. Phys. A 627 (1997) 495. URL: <https://www.sciencedirect.com/science/article/pii/S0375947497005988>. doi:10.1016/S0375-9474(97)00598-8.
- [38] T. Nikšić, D. Vretenar, P. Ring, Phys. Rev. C 78 (2008) 034318. URL: <https://link.aps.org/doi/10.1103/PhysRevC.78.034318>. doi:10.1103/PhysRevC.78.034318.
- [39] J. Zhao, B.-N. Lu, E.-G. Zhao, S.-G. Zhou, Phys. Rev. C 95 (2017) 014320. URL: <https://link.aps.org/doi/10.1103/PhysRevC.95.014320>. doi:10.1103/PhysRevC.95.014320.
- [40] E. Yüksel, T. Marketin, N. Paar, Phys. Rev. C 99 (2019) 034318. URL: <https://link.aps.org/doi/10.1103/PhysRevC.99.034318>. doi:10.1103/PhysRevC.99.034318.
- [41] A. Taninah, S. E. Agbemava, A. V. Afanasjev, P. Ring, Phys. Lett. B 800 (2020) 135065. URL: <https://www.sciencedirect.com/science/article/pii/S0370269319307877>. doi:10.1016/j.physletb.2019.135065.
- [42] U. C. Perera, A. V. Afanasjev, P. Ring, Phys. Rev. C 104 (2021) 064313. URL: <https://link.aps.org/doi/10.1103/PhysRevC.104.064313>. doi:10.1103/PhysRevC.104.064313.
- [43] D. Vale, Y. F. Niu, N. Paar, Phys. Rev. C 103 (2021) 064307. URL: <https://link.aps.org/doi/10.1103/PhysRevC.103.064307>. doi:10.1103/PhysRevC.103.064307.
- [44] F. Ji, J. Hu, H. Shen, Phys. Rev. C 103 (2021) 055802. URL: <https://link.aps.org/doi/10.1103/PhysRevC.103.055802>. doi:10.1103/PhysRevC.103.055802.
- [45] K. Zhang, M.-K. Cheoun, Y.-B. Choi, P. S. Chong, J. Dong, Z. Dong, X. Du, L. Geng, E. Ha, X.-T. He, C. Heo, M. C. Ho, E. J. In, S. Kim, Y. Kim, C.-H. Lee, J. Lee, H. Li, Z. Li, T. Luo, J. Meng, M.-H. Mun, Z. Niu, C. Pan, P. Papakonstantinou, X. Shang, C. Shen, G. Shen, W. Sun, X.-X. Sun, C. K. Tam, Thavayongnou, C. Wang, X. Wang, S. H. Wong, J. Wu, X. Wu, X. Xia, Y. Yan, R. W.-Y. Yeung, T. C. Yiu, S. Zhang, W. Zhang, X. Zhang, Q. Zhao, S.-G. Zhou, At. Data Nucl. Data Tables 144 (2022) 101488. URL: <https://www.sciencedirect.com/science/article/pii/S0092640X22000018>. doi:10.1016/j.adt.2022.101488.
- [46] Y. Tian, Z. Y. Ma, P. Ring, Phys. Lett. B 676 (2009) 44. URL: <https://www.sciencedirect.com/science/article/pii/S0370269309004912>. doi:10.1016/j.physletb.2009.04.067.
- [47] Y. Tian, Z.-y. Ma, P. Ring, Phys. Rev. C 79 (2009) 064301. URL: <https://link.aps.org/doi/10.1103/PhysRevC.79.064301>. doi:10.1103/PhysRevC.79.064301.
- [48] A. V. Afanasjev, O. Abdurazakov, Phys. Rev. C 88 (2013) 014320. URL: <https://link.aps.org/doi/10.1103/PhysRevC.88.014320>. doi:10.1103/PhysRevC.88.014320.
- [49] P. Ring, P. Schuck, The Nuclear Many-body Problem, Springer-Verlag, 1980.
- [50] J. F. Berger, M. Girod, D. Gogny, Nucl. Phys. A 428 (1984) 23. URL: <https://www.sciencedirect.com/science/article/pii/0375947484902409>. doi:10.1016/0375-9474(84)90240-9.
- [51] M. Bender, K. Rutz, P. G. Reinhard, J. A. Maruhn, Eur. Phys. J. A. 8 (2000) 59. URL: <https://doi.org/10.1007/s10050-000-4504-z>. doi:10.1007/s10050-000-4504-z.
- [52] X. W. Xia, Y. Lim, P. W. Zhao, H. Z. Liang, X. Y. Qu, Y. Chen, H. Liu, L. F. Zhang, S. Q. Zhang, Y. Kim, J. Meng, At. Data Nucl. Data Tables 121 (2018) 1. URL: <https://www.sciencedirect.com/science/article/pii/S0092640X17300451>. doi:10.1016/j.adt.2017.09.001.
- [53] I. Angeli, K. Marinova, At. Data Nucl. Data Tables 99 (2013) 69. URL: <https://www.sciencedirect.com/science/article/pii/S0092640X12000265>. doi:10.1016/j.adt.2011.12.006.
- [54] D. Adhikari, H. Albatineh, D. Androic, K. Aniol, D. S. Armstrong, T. Averett, C. Ayerbe Gayoso, S. Barcus, V. Bellini, R. S. Beminiwattha, J. F. Benesch, H. Bhatt, D. Bhatta Pathak, D. Bhetuwal, B. Blaikie, Q. Campagna, A. Camsonne, G. D. Cates, Y. Chen, C. Clarke, J. C. Cornejo, S. Covrig Dusa, P. Datta, A. Deshpande, D. Dutta, C. Feldman, E. Fuchey, C. Gal, D. Gaskell, T. Gautam, M. Gericke, C. Ghosh, I. Halilovic, J.-O. Hansen, F. Hauenstein, W. Henry, C. J. Horowitz, C. Jantzi, S. Jian, S. Johnston, D. C. Jones, B. Karki, S. Katugampola, C. Keppel, P. M. King, D. E. King, M. Knauss, K. S. Kumar, T. Kutz, N. Lashley-Colthirst, G. Leverick, H. Liu, N. Liyange, S. Malace, R. Mammeei, J. Mammeei, M. McCaughan, D. McNulty, D. Meekins, C. Metts, R. Michaels, M. M. Mondal, J. Napolitano, A. Narayan, D. Nikolaev, M. N. H. Rashad, V. Owen, C. Palatchi, J. Pan, B. Pandey, S. Park, K. D. Paschke, M. Petrusky, M. L. Pitt, S. Premathilake, A. J. R. Puckett, B. Quinn, R. Radloff, S. Rahman, A. Rathnayake, B. T. Reed, P. E. Reimer, R. Richards, S. Riordan, Y. Roblin, S. Seeds, A. Shahinyan, P. Souder, L. Tang, M. Thiel, Y. Tian, G. M. Urciuoli, E. W. Wertz, B. Wojtsekhowski, B. Yale, T. Ye, A. Yoon, A. Zec, W. Zhang, J. Zhang, X. Zheng (PREX Collaboration), Phys. Rev. Lett. 126 (2021) 172502. URL: <https://link.aps.org/doi/10.1103/PhysRevLett.126.172502>. doi:10.1103/PhysRevLett.126.172502.
- [55] R. Brockmann, R. Machleidt, Phys. Rev. C 42 (1990) 1965. URL: <https://link.aps.org/doi/10.1103/PhysRevC.42.1965>. doi:10.1103/PhysRevC.42.1965.
- [56] F. G. Kondev, M. Wang, W. J. Huang, S. Naimi, G. Audi, Chin. Phys. C 45 (2021) 030001. URL: <https://doi.org/10.1088/1674-1137/abddae>. doi:10.1088/1674-1137/abddae.
- [57] M. Anguiano, J. Egido, L. Robledo, Nucl. Phys. A 683 (2001) 227. URL: <https://www.sciencedirect.com/science/article/pii/S0375947400004450>. doi:https://doi.org/10.1016/S0375-9474(00)00445-0.
- [58] I. Borzov, Nucl. Phys. A 777 (2006) 645. URL: <https://www.sciencedirect.com/science/article/pii/S0375947405008511>. doi:https://doi.org/10.1016/j.nuclphysa.2005.05.147.

- [59] A. Manohar, H. Georgi, Nucl. Phys. B 234 (1984) 189. URL: <https://www.sciencedirect.com/science/article/pii/0550321384902311>. doi:[https://doi.org/10.1016/0550-3213\(84\)90231-1](https://doi.org/10.1016/0550-3213(84)90231-1).
- [60] M. Bender, K. Rutz, P. Reinhard, J. Maruhn, Eur. Phys. J. A 8 (2000) 59. URL: <https://doi.org/10.1007/s10050-000-4504-z>. doi:<https://doi.org/10.1007/s10050-000-4504-z>.
- [61] A. Akmal, V. R. Pandharipande, D. G. Ravenhall, Phys. Rev. C 58 (1998) 1804. URL: <https://link.aps.org/doi/10.1103/PhysRevC.58.1804>. doi:[10.1103/PhysRevC.58.1804](https://doi.org/10.1103/PhysRevC.58.1804).
- [62] B. Kłos, A. Trzcińska, J. Jastrzębski, T. Czosnyka, M. Kisieliński, P. Lubiński, P. Napiorkowski, L. Pieńkowski, F. J. Hartmann, B. Ketzner, P. Ring, R. Schmidt, T. v. Egidy, R. Smolańczuk, S. Wycech, K. Gulda, W. Kurcewicz, E. Widmann, B. A. Brown, Phys. Rev. C 76 (2007) 014311. URL: <https://link.aps.org/doi/10.1103/PhysRevC.76.014311>. doi:[10.1103/PhysRevC.76.014311](https://doi.org/10.1103/PhysRevC.76.014311).
- [63] A. Klimkiewicz, N. Paar, P. Adrich, M. Fallot, K. Boretzky, T. Aumann, D. Cortina-Gil, U. D. Pramanik, T. W. Elze, H. Emling, H. Geissel, M. Hellström, K. L. Jones, J. V. Kratz, R. Kulesa, C. Nociforo, R. Palit, H. Simon, G. Surówka, K. Sümmerer, D. Vretenar, W. Waluś (LAND Collaboration), Phys. Rev. C 76 (2007) 051603. URL: <https://link.aps.org/doi/10.1103/PhysRevC.76.051603>. doi:[10.1103/PhysRevC.76.051603](https://doi.org/10.1103/PhysRevC.76.051603).
- [64] J. Zenihiro, H. Sakaguchi, T. Murakami, M. Yosoi, Y. Yasuda, S. Terashima, Y. Iwao, H. Takeda, M. Itoh, H. P. Yoshida, M. Uchida, Phys. Rev. C 82 (2010) 044611. URL: <https://link.aps.org/doi/10.1103/PhysRevC.82.044611>. doi:[10.1103/PhysRevC.82.044611](https://doi.org/10.1103/PhysRevC.82.044611).
- [65] A. Tamii, I. Poltoratska, P. von Neumann-Cosel, Y. Fujita, T. Adachi, C. A. Bertulani, J. Carter, M. Dozono, H. Fujita, K. Fujita, K. Hatanaka, D. Ishikawa, M. Itoh, T. Kawabata, Y. Kalmykov, A. M. Krumbholz, E. Litvinova, H. Matsubara, K. Nakanishi, R. Neveling, H. Okamura, H. J. Ong, B. Özel-Tashenov, V. Y. Ponomarev, A. Richter, B. Rubio, H. Sakaguchi, Y. Sakemi, Y. Sasamoto, Y. Shimbara, Y. Shimizu, F. D. Smit, T. Suzuki, Y. Tameshige, J. Wambach, R. Yamada, M. Yosoi, J. Zenihiro, Phys. Rev. Lett. 107 (2011) 062502. URL: <https://link.aps.org/doi/10.1103/PhysRevLett.107.062502>. doi:[10.1103/PhysRevLett.107.062502](https://doi.org/10.1103/PhysRevLett.107.062502).
- [66] C. M. Tarbert, D. P. Watts, D. I. Glazier, P. Aguar, J. Ahrens, J. R. M. Annand, H. J. Arends, R. Beck, V. Bekrenev, B. Boillat, A. Braghieri, D. Branford, W. J. Briscoe, J. Brudvik, S. Cherepnaya, R. Codling, E. J. Downie, K. Foehl, P. Grabmayr, R. Gregor, E. Heid, D. Hornidge, O. Jahn, V. L. Kashevarov, A. Knezevic, R. Kondratiev, M. Korolija, M. Kotulla, D. Krambrich, B. Krusche, M. Lang, V. Lisin, K. Livingston, S. Lugert, I. J. D. MacGregor, D. M. Manley, M. Martinez, J. C. McGeorge, D. Mekerovic, V. Metag, B. M. K. Nefkens, A. Nikolaev, R. Novotny, R. O. Owens, P. Pedroni, A. Polonski, S. N. Prakhov, J. W. Price, G. Rosner, M. Rost, T. Rostomyan, S. Schadmand, S. Schumann, D. Sober, A. Starostin, I. Supek, A. Thomas, M. Unverzagt, T. Walcher, L. Zana, F. Zehr (Crystal Ball at MAMI and A2 Collaboration), Phys. Rev. Lett. 112 (2014) 242502. URL: <https://link.aps.org/doi/10.1103/PhysRevLett.112.242502>. doi:[10.1103/PhysRevLett.112.242502](https://doi.org/10.1103/PhysRevLett.112.242502).
- [67] C. D. Pruitt, R. J. Charity, L. G. Sobotka, M. C. Atkinson, W. H. Dickhoff, Phys. Rev. Lett. 125 (2020) 102501. URL: <https://link.aps.org/doi/10.1103/PhysRevLett.125.102501>. doi:[10.1103/PhysRevLett.125.102501](https://doi.org/10.1103/PhysRevLett.125.102501).
- [68] Q. Zhao, Z. X. Ren, P. W. Zhao, J. Meng, Phys. Rev. C 106 (2022) 034315. URL: <https://link.aps.org/doi/10.1103/PhysRevC.106.034315>. doi:[10.1103/PhysRevC.106.034315](https://doi.org/10.1103/PhysRevC.106.034315).

Supplementary Material

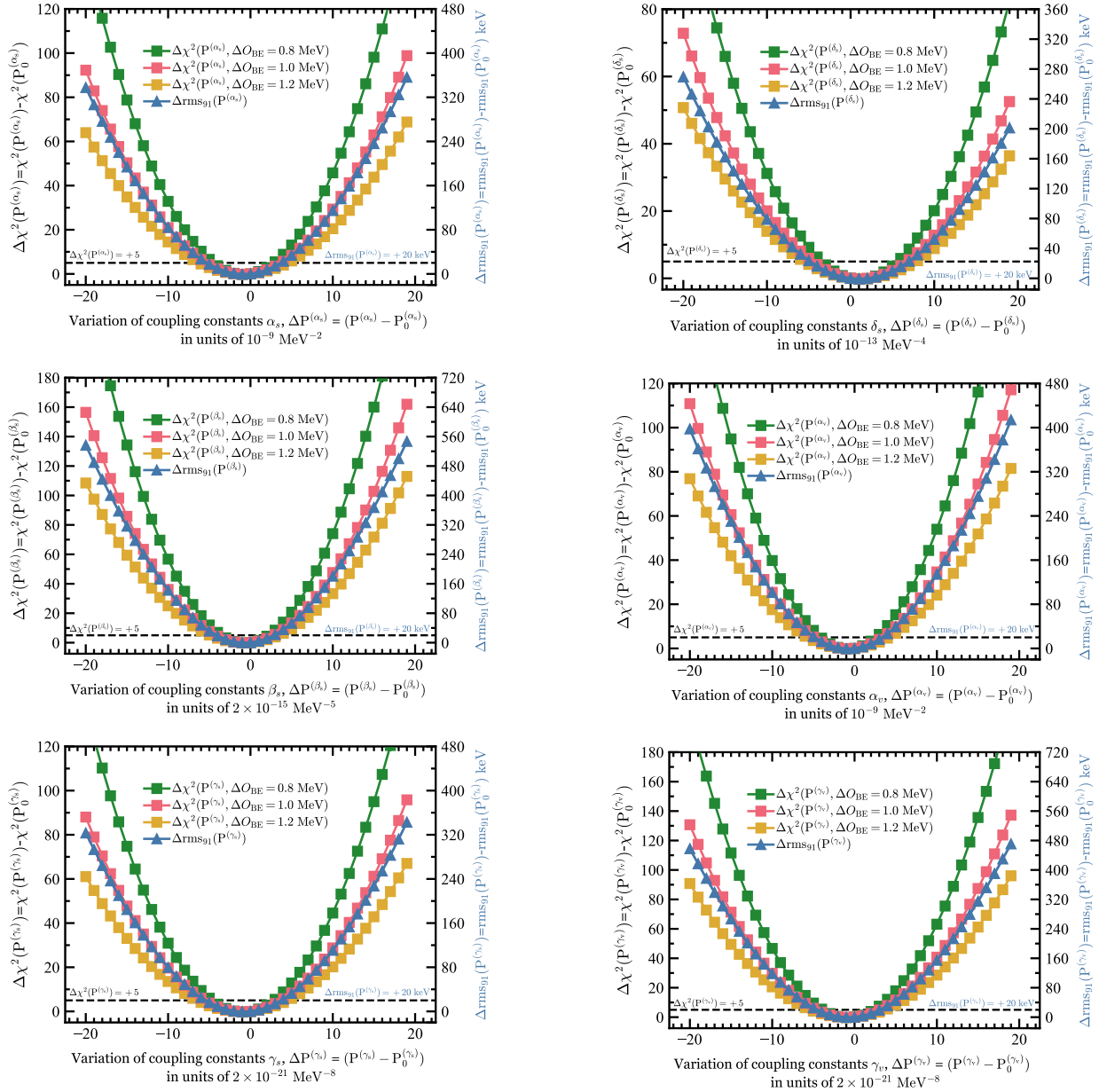


Figure S1a: The variation of the coupling constants corresponding to the local minima obtained by the χ^2 -minimization (green, red, and yellow squares) and the rms of 91 spherical nuclei binding energies (blue triangles) for the relativistic density functional PC-L3R. The optimal parametrization is found for the parameter set P_0 corresponding to the minimum of the penalty function $\chi^2(P_0)$. Each x-axis indicates the parameter variations, ΔP , from the P_0 at the respective local minima. Each left y-axis shows the $\chi^2(P)$ deviations, $\Delta\chi^2(P)$, from the $\chi^2(P_0)$ at the respective local minima. Each right y-axis displays the rms deviations, $\Delta\text{rms}_{91}(P)$, due to the variations of the respective parameter from the optimized $\text{rms}_{91}(P_0)$. Three sets of ΔO_{BE} theoretical weights are studied to perceive the influence of the defined weight on the optimization. The $\Delta\chi^2$ based on $\Delta O_{\text{BE}} = 0.8$ MeV, 1 MeV, and 1.2 MeV are indicated as green, red, and yellow squares, respectively. The blue dash line is the constraint at $\Delta\text{rms}_{91} \lesssim 20$ keV, for defining the parameter uncertainties. This figure set illustrates the optimizations of point-coupling constants, α_S (top panel), β_S (middle panel), and γ_S (bottom panel). See Figs. S1b, S1c, and S1d for optimizations of other parameters.

Figure S1b: The optimizations of point-coupling constants, δ_S (top panel), α_V (middle panel), and γ_V (bottom panel). See Figs. S1a, S1c, and S1d for optimizations of other parameters. For further description, see Fig. S1a.

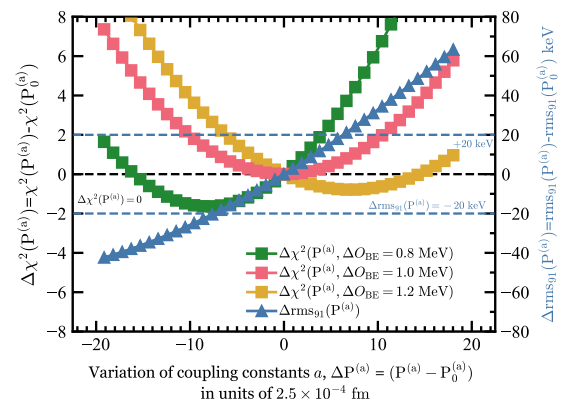
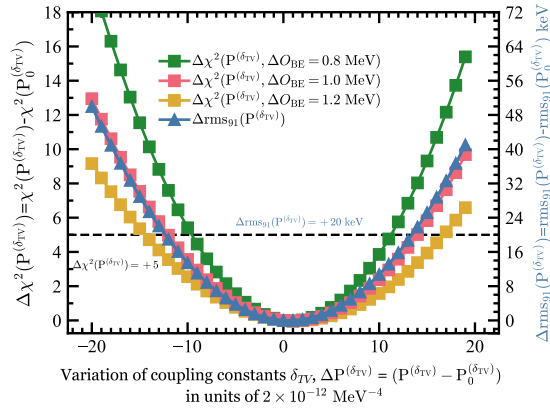
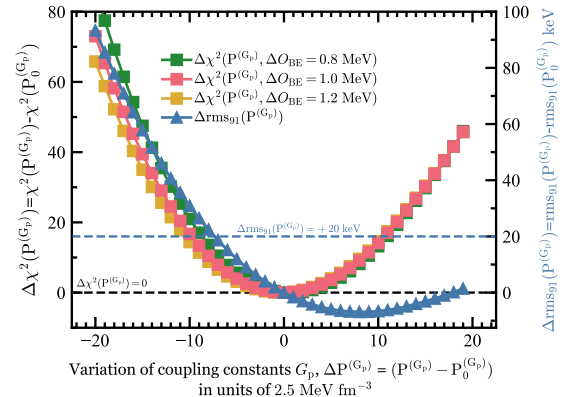
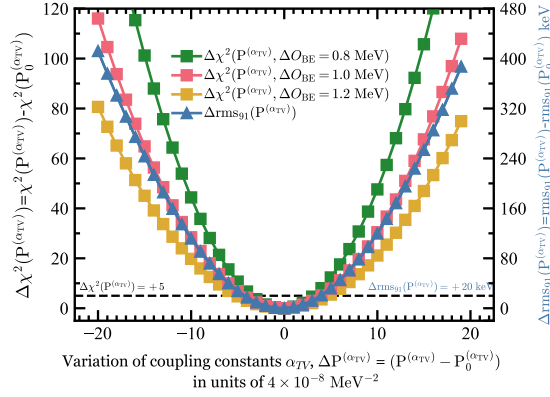
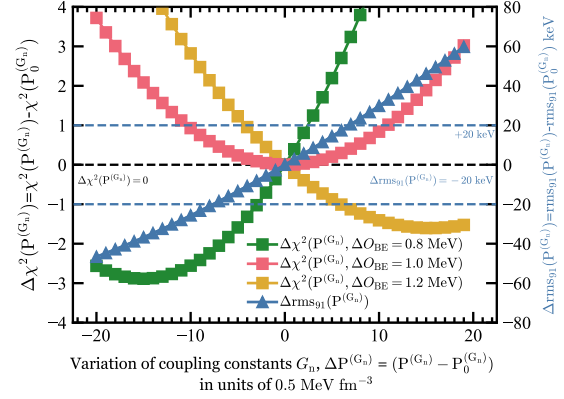
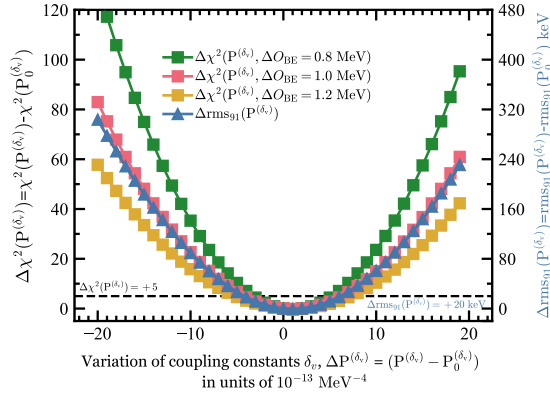


Figure S1c: The optimizations of point-coupling constants, δ_V (top panel), α_{TV} (middle panel), and δ_{TV} (bottom panel). See Figs. S1a, S1b, and S1d for optimizations of other parameters. For further description, see Fig. S1a. With referring to the results presented in Figs. S1a, S1b, and S1c, the variations of ΔO_{BE} do not affect the local minima of point-coupling constants, i.e., $\Delta\chi^2(P_0)$ and $\Delta rms_{91}(P_0)$. Therefore, assuming $\Delta O_{BE} = 1$ MeV is justified and in accord with the definition of previous works [19, 38, 40, 41]. The influence of variations in ΔO_{BE} on the local minima of pairing strengths and a factor is given in Fig. S1d.

Figure S1d: The optimizations of G_n (top panel) and G_p (middle panel) pairing strengths, and a factor (bottom panel). See Figs. S1a, S1b, and S1c for optimizations of other parameters. For further description, see Fig. S1a. The local minima of the G_n pairing strength, $\Delta\chi^2(P_0^{(G_n)})$, and a factor, $\Delta\chi^2(P_0^{(a)})$, and the corresponding $\Delta rms_{91}^{(G_n)}$ and $\Delta rms_{91}^{(a)}$, are varied accordingly with variations in ΔO_{BE} . Nevertheless, the influence of ΔO_{BE} variations on the $\Delta\chi^2(P^{(G_p)})$ corresponding to the G_p pairing strength is negligible. Meanwhile, the rms values of mean pairing gaps, rms_{PG} , are inversely varied accordingly with variations in ΔO_{BE} as well, i.e., for the pairing strength G_n , $rms_{PG} = 0.237$ MeV ($\Delta O_{BE} = 0.8$ MeV), $rms_{PG} = 0.217$ MeV ($\Delta O_{BE} = 1$ MeV), $rms_{PG} = 0.196$ MeV ($\Delta O_{BE} = 1.2$ MeV), and for the a factor, $rms_{PG} = 0.228$ MeV ($\Delta O_{BE} = 0.8$ MeV), $rms_{PG} = 0.217$ MeV ($\Delta O_{BE} = 1$ MeV), $rms_{PG} = 0.208$ MeV ($\Delta O_{BE} = 1.2$ MeV). Therefore, it is still appropriate to define $\Delta O_{BE} = 1$ MeV for a balance weight to constrain the point-coupling interaction.

Table S1

The coupling constants and penalty function χ^2 of the non-linear point-coupling interaction PC-L3R, PC-F1, PC-PK1, and PC-X. The separable pairing force (modeled D1S) is implemented in the PC-F1, PC-PK1, and PC-X interactions.

	PC-L3R	PC-X	PC-PK1	PC-F1
α_S (MeV ⁻²)	-3.99289×10^{-04}	-4.0242×10^{-04}	-3.96291×10^{-04}	-3.83577×10^{-04}
β_S (MeV ⁻⁵)	8.65504×10^{-11}	8.5958×10^{-11}	8.6653×10^{-11}	7.68567×10^{-11}
γ_S (MeV ⁻⁸)	-3.83950×10^{-17}	-3.7304×10^{-17}	-3.80724×10^{-17}	-2.90443×10^{-17}
δ_S (MeV ⁻⁴)	-1.20749×10^{-10}	-0.52181×10^{-10}	-1.09108×10^{-10}	-4.1853×10^{-10}
α_V (MeV ⁻²)	2.71991×10^{-04}	2.7534×10^{-04}	2.6904×10^{-04}	2.59333×10^{-04}
γ_V (MeV ⁻⁸)	-3.72107×10^{-18}	-4.9012×10^{-18}	-3.64219×10^{-18}	-3.879×10^{-18}
δ_V (MeV ⁻⁴)	-4.26653×10^{-10}	-5.9440×10^{-10}	-4.32619×10^{-10}	-1.1921×10^{-10}
α_{TV} (MeV ⁻²)	2.96688×10^{-05}	2.8188×10^{-05}	2.95018×10^{-05}	3.4677×10^{-05}
δ_{TV} (MeV ⁻⁴)	-4.65682×10^{-10}	-5.2838×10^{-10}	-4.11112×10^{-10}	-4.2×10^{-11}
χ^2	274.478	494.875	364.449	751.225

The Justification of the Point-Coupling Interaction,

PC-L3R – Table S1 shows the coupling constants and penalty functions of the point-coupling interactions PC-L3R, PC-F1, PC-PK1, and PC-X, obtained from Eq. (18). Referring to the work of Manohar and Georgi [59], we can scale the newly optimized coupling constants in the point-coupling interaction to a generic QCD-based Lagrangian term using the expression,

$$\mathcal{L} \sim -c_{ln} \left[\frac{\bar{\psi}\psi}{f_\pi^2 \Lambda} \right]^l \left[\frac{\partial^\mu}{\Lambda} \right]^n f_\pi^2 \Lambda^2, \quad (19)$$

where ψ is the nucleon field, f_π is the pion decay constants, $\Lambda = 770$ MeV is a generic QCD large-mass scale. The chiral symmetry in weakening the N-body forces demands $\Delta = l+n-2 \geq 0$. By scaling the coupling constants in accordance with the QCD-based Lagrangian, the naturalness in effective theories can be justified. If the theory is natural, the Lagrangian should lead to dimensionless coefficients c_{ln} within numerical factors of the order of unity [19, 23]. The corresponding QCD-scaled coupling constants c_{ln} for each coupling constants of the relativistic point-coupling interactions PC-L3R, PC-F1, PC-PK1, and PC-X are presented in Table S2. The numerical values of these corresponding QCD-scaled coupling constants c_{ln} indicate that the nine coupling constants of the PC-L3R, PC-F1, PC-PK1, and PC-X interactions are natural.

Table S2

The corresponding QCD-scaled coupling constants c_{ln} to each coupling constants of the point-coupling interactions PC-L3R, PC-F1, PC-PK1, and PC-X.

	c_{ln} (PC-L3R)	c_{ln} (PC-X)	c_{ln} (PC-PK1)	c_{ln} (PC-F1)
α_S	-1.708	-1.722	-1.695	-1.641
β_S	1.626	1.615	1.628	1.443
γ_S	-3.565	-3.464	-3.535	-2.695
δ_S	-0.306	-0.132	-0.277	-1.061
α_V	1.164	1.178	1.151	1.109
γ_V	-0.345	-0.455	-0.338	-0.360
δ_V	-1.082	-1.508	-1.097	-0.302
α_{TV}	0.508	0.482	0.505	0.593
δ_{TV}	-4.725	-5.361	-4.171	-0.426

The Constraint of Pairing Interaction – We further optimize the separable pairing force, of which the G pairing strength is separated to the neutron (G_n) and proton (G_p) pairing strengths to improve the description of the finite nuclear properties. An empirical pairing gap, based on the five-point formula [60], is expressed as

$$\Delta_q^{(5)}(N_0) = -\frac{\pi_{N_0}}{8} [E(N_0 + 2) - 4E(N_0 + 1) + 6E(N_0) - 4E(N_0 - 1) + E(N_0 - 2)], \quad (20)$$

where N_0 is either the proton (or neutron) number of a selected nucleus, $\pi_{N_0} = -1^{N_0}$ is the number parity, and $E(N_0)$ is the binding energy of the selected nucleus. For the present work, we consider twelve sets of mean pairing gaps consisting of 54 nuclei in total, of which the N_0 nuclei are: ⁸⁴Se, ⁸⁸Sr, ⁹²Mo, ¹¹²Sn, ¹¹⁸Sn, ¹²⁴Sn, ¹³⁸Ba, ¹⁴²Nd, ¹⁴⁶Gd, ²⁰⁴Pb, ²¹²Rn, and ²¹⁴Ra.

The rms value of comparing experimental and theoretical pairing gaps produced from the PC-L3R interaction used in RHB model with a further optimized separable pairing interaction is 0.217 MeV, whereas the rms values yielded from the PC-X, PC-PK1*, DD-PCX, and DD-PC1* are 0.109 MeV, 0.124 MeV, 0.273 MeV, and 0.115 MeV, respectively. These mean pairing gaps are exhibited in Fig. S4. We remark that the ΔO_{PG} weight can be defined as either 0.1 MeV or 0.05 MeV for Eq. (18). Defining $\Delta O_{PG} = 0.05$ MeV can somehow impose a reduction of ~ 70 keV on the rms of pairing gap. Nevertheless, such reduction of rms does not significantly alter the theoretical mean pairing gaps. Therefore, defining $\Delta O_{PG} = 0.1$ MeV is rather appropriate to reduce both rms values of mean pairing gaps and binding energies.

The Symmetric Nuclear Matter Energy – Figure S3 displays the binding energy curves for symmetric nuclear matter produced from the PC-L3R, PC-PK1, PC-X, DD-PC1, DD-PCX, PC-F1, and PC-LA interactions, and the *ab initio* variational calculations (black dots) [61]. For the baryon density $\rho_B \leq 0.20$, the E/A predicted by PC-L3R is consistent with all point-coupling interactions and the *ab initio* variational calculation owing to the constraints from the properties of finite nuclei. For the high density region with

Table S3

(continued)

Nuclei	AME2020	PC-L3R ^a	PC-PK1 ^b	PC-PK1 ^c	PC-PK1 ^{*,d}	PC-X ^e	DD-PC1 ^f	DD-PC1 ^{*,g}	DD-PCX ^h	PC-F1 ⁱ	PC-F1 ^{*,j}	PC-LA ^k	PC-LA ^{*,l}
¹⁹⁸ Pb	-1560.036	-1558.433	-1558.218	-1557.214	-1555.71	-1556.029	-1561.123	-1559.500	-1557.703	-1559.292	-1560.242	-1559.829	-1558.650
²⁰⁰ Pb	-1576.362	-1574.998	-1574.885	-1574.075	-1572.71	-1572.996	-1577.817	-1576.520	-1574.578	-1575.666	-1576.532	-1575.769	-1574.841
²⁰² Pb	-1592.195	-1591.163	-1591.172	-1590.601	-1589.49	-1589.639	-1594.139	-1593.212	-1591.079	-1591.675	-1592.448	-1591.240	-1590.592
²⁰⁴ Pb	-1607.506	-1606.896	-1607.068	-1606.765	-1606.05	-1605.928	-1610.026	-1609.526	-1607.165	-1607.325	-1607.963	-1606.187	-1605.845
²⁰⁶ Pb	-1622.325	-1622.133	-1622.525	-1622.498	-1622.32	-1621.784	-1625.385	-1625.335	-1622.743	-1622.563	-1623.014	-1620.490	-1620.454
²⁰⁸ Pb	-1636.430	-1636.735	-1637.438	-1637.626	-1637.92	-1637.004	-1640.008	-1640.281	-1637.578	-1637.241	-1637.442	-1633.865	-1633.990
²¹⁰ Pb	-1645.553	-1645.180	-1645.449	-1645.684	-1645.59	-1644.936	-1648.272	-1648.032	-1644.993	-1644.793	-1645.397	-1641.484	-1641.006
²¹² Pb	-1654.516	-1653.439	-1653.425	-1653.658	-1653.19	-1652.803	-1656.428	-1655.716	-1652.275	-1652.275	-1652.275	-1653.182	-1648.887
²¹⁴ Pb	-1663.293	-1661.535	-1661.397	-1661.552	-1660.73	-1660.609	-1664.481	-1663.324	-1659.437	-1659.697	-1660.804	-1656.073	-1654.660
²¹⁰ Po	-1645.213	-1646.217	-1646.703	-1647.137	-1647.25	-1646.206	-1649.441	-1649.855	-1646.732	-1647.760	-1648.346	-1644.643	-1644.878
²¹² Rn	-1652.497	-1654.242	-1654.632	-1655.131	-1655.11	-1653.940	-1657.476	-1657.930	-1654.342	-1654.342	-1654.342	-1653.921	-1654.215
²¹⁴ Ra	-1658.323	-1660.831	-1661.172	-1661.643	-1661.55	-1660.229	-1664.092	-1664.540	-1660.438	-1664.512	-1665.213	-1661.709	-1662.043
²¹⁶ Th	-1662.695	-1665.941	-1666.248	-1666.633	-1666.59	-1665.027	-1669.244	-1669.659	-1664.982	-1670.649	-1671.232	-1667.967	-1668.335
²¹⁸ U	-1665.677	-1669.317	-1669.602	-1669.847	-1670.05	-1668.086	-1672.733	-1673.060	-1668.816	-1675.109	-1675.372	-1672.491	-1672.882
rms₆₀^m		1.176	1.248	1.417	1.64	1.378	3.139	3.269	1.413	2.589	2.913	2.581	2.890
rms₆₅ⁿ		1.245	1.312	1.495	1.69	1.542	3.088	3.206	1.461	2.590	2.895	2.615	2.914
rms₉₁^o		1.339	1.453	1.796	2.11	2.168	2.805	2.925	1.712	2.493	2.755	2.555	2.714
rrs₆₀		0.22%	0.18%	0.22%	0.39%	0.20%	0.47%	0.50%	0.22%	0.30%	0.39%	0.29%	0.34%
rrs₆₅		0.23%	0.19%	0.23%	0.39%	0.22%	0.45%	0.49%	0.23%	0.32%	0.40%	0.30%	0.35%
rrs₉₁		0.24%	0.23%	0.27%	0.39%	0.27%	0.44%	0.48%	0.26%	0.35%	0.40%	0.32%	0.35%

The experimental binding energies compiled in AME2020 [56]. ^a PC-L3R: calculated from the RHB model with the PC-L3R interaction. ^b PC-PK1: quoted from the RMF model with the Bardeen-Cooper-Schrieffer (BCS) theory using the PC-PK1 interaction [19] and δ pairing force. ^c PC-PK1^{*}: calculated from the RHB model using the PC-PK1 interaction [19] and separable pairing force [46]. ^d PC-PK1[†]: quoted from the relativistic continuum Hartree-Bogoliubov (RCHB) model [52] using the PC-PK1 interaction [19] and δ pairing force. ^e PC-X: calculated from the RHB model using the PC-X interaction [41] and separable pairing force [46]. ^f DD-PC1: quoted from the RMF model with the BCS theory using the DD-PC1 interaction [38] and δ pairing force. ^g DD-PC1^{*}: calculated from the RHB model using the DD-PC1 interaction [38] and separable pairing force [46]. ^h DD-PCX: calculated from the RHB model using the DD-PCX interaction [40] and separable pairing force [46]. ⁱ PC-F1: quoted from the RMF model with the BCS theory using the PC-F1 interaction [23] and δ pairing force. ^j PC-F1^{*}: calculated from the RHB model using the PC-F1 interaction [23] and separable pairing force [46]. ^k PC-LA: quoted from the RMF model with the BCS theory using the PC-LA interaction [36] and δ pairing force. ^l PC-LA^{*}: calculated from the RHB model using the PC-LA interaction [36] and separable pairing force [46]. The root mean square (rms) and the root of relative square (rrs) deviations of comparing the theoretical and experimental binding energies are listed in the last rows. ^m rms₆₀: calculated from the binding energies of 60 spherical nuclei (black bold texts), selected for fitting the PC-PK1 [39]. ⁿ rms₆₅: calculated from the binding energies of 65 spherical nuclei (blue bold texts), referred by previous works in fitting point coupling interactions [19, 40, 41]. ^o rms₉₁: calculated from the binding energies of 91 spherical nuclei (all nuclei in this table), selected for the present work fitting the PC-L3R interaction. The rrs have a similar label as rms.

$\rho_B \geq 0.30$, the DD-PCX binding energy curve is closer to the prediction from the *ab initio* variational calculation, while softer than those from the PC-L3R, PC-PK1, PC-X, and PC-F1 interactions, and stiffer than the one from the DD-PC1, and PC-LA interactions. Note that the inconsistent description at the high-density nuclear matter region, $\rho_B \geq 0.30$, is not sensitive on the description of the low-energy bulk nuclear properties.

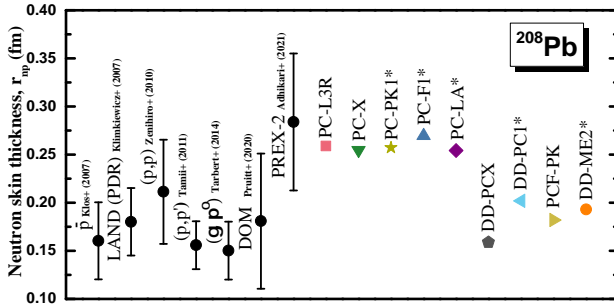


Figure S2: The neutron skin thickness for ²⁰⁸Pb determined by experiments and predicted by nuclear energy density functionals. The experimental data are taken from \bar{p} [62], LAND(PDR) [63], (*p, p*) [64], (*p, p'*) [65], (γ, π^0) [66], and PREX-2 [54]. The calculations are based on the frameworks PC-L3R, PC-X, PC-PK1^{*}, PC-F1^{*}, PC-LA^{*}, DD-PCX, DD-PC1^{*}, and DD-ME2^{*}, described in the footnotes of Tables 2 and S3. The result of PCF-PK1 is quoted from with Zhao et al. [68].

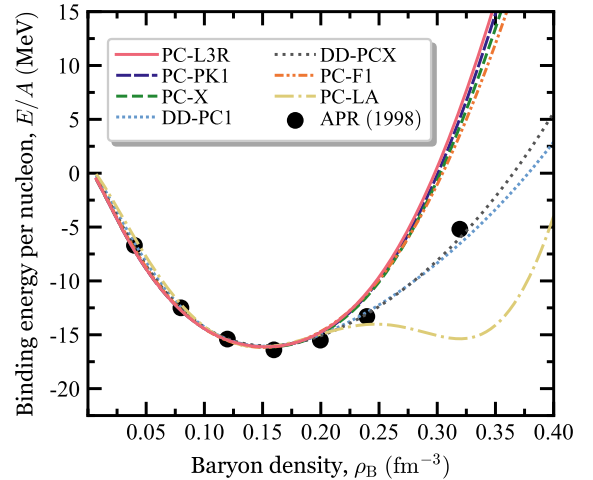


Figure S3: The binding energy per nucleon, E/A , for the nuclear matter as a function of the baryon density, ρ_B , see texts.

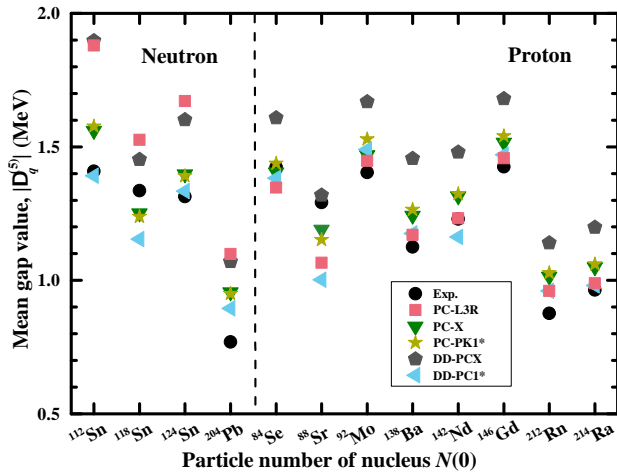


Figure S4: The five-point mean pairing gap values from AME2020 and present calculations using the frameworks of PC-L3R, PC-X, PC-PK1*, DD-PCX, and DD-PC1*. See the footnotes of Tables 2 and S3 for the description of these frameworks. The left panel shows the neutron mean gap values whereas the right panel illustrates the proton mean gap values.

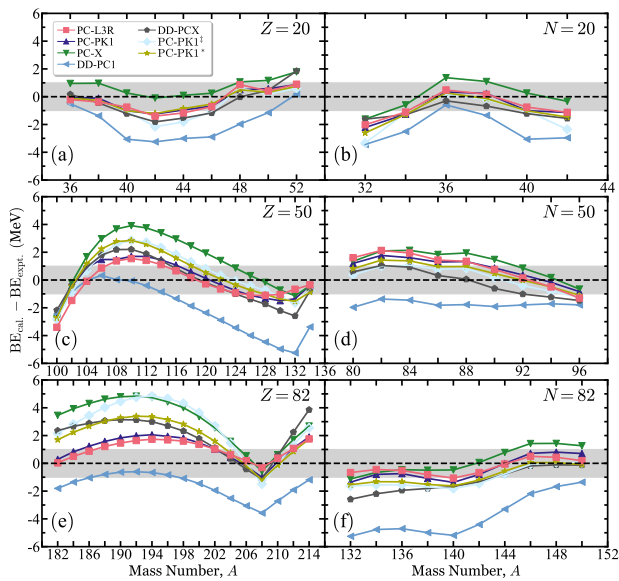


Figure S5: The deviations between the AME2020 experimental data [56] and the calculated binding energies for the $Z = 20, 50,$ and 82 isotopes, and for the $N = 20, 50,$ and 82 isotones. See the footnote of Tables 2 and S3 for the theoretical frameworks in this figure. The data of PC-PK1 (black triangles) and DD-PC1 (blue squares) are from Ref. [19], whereas the PC-PK1* data is from Ref. [52].

Table S4
The comparison of charge radii (in fm) of the selected 63 spherical nuclei.

Nuclei	Expt.	PC-L3R ^a	PC-PK1 ^b	PC-PK1 ^{ac}	PC-PK1 ^{ad}	PC-X ^e	DD-PC1 ^f	DD-PC1 ^{g*}	DD-PCX ^h	PC-F1 ⁱ	PC-F1 ^{aj}	PC-LA ^k	PC-LA ^{al}
¹⁶ O	2.6991	2.7676	2.7677	2.7677	2.768	2.7698	2.7472	2.7471	2.7594	2.7633	2.7632	2.7528	2.7528
¹⁸ O	2.7726	2.7599		2.7594	2.763	2.7603		2.7475	2.7622		2.7563		2.7505
¹⁸ Ne	2.9714	2.9694		2.9700	2.960	2.9691		2.9456	2.9564		2.9693		2.9508
³⁶ S	3.2985	3.2852		3.2872	3.289	3.2904		3.2898	3.2926		3.2912		3.3016
³⁸ Ar	3.4028	3.3918		3.3916	3.391	3.3942		3.3785	3.3837		3.3903		3.3891
⁴⁰ Ca	3.4776	3.4826	3.4815	3.4814	3.481	3.4832	3.4566	3.4561	3.4617	3.4777	3.4774	3.4678	3.4674
⁴² Ca	3.5081	3.4821	3.4805	3.4808	3.482	3.4820	3.4626	3.4622	3.4689	3.4778	3.4782	3.4729	3.4725
⁴⁴ Ca	3.5179	3.4848	3.4826	3.4832	3.486	3.4838	3.4709	3.4705	3.4777	3.4809	3.4817	3.4810	3.4806
⁴⁶ Ca	3.4953	3.4890	3.4865	3.4869	3.490	3.4871	3.4806	3.4799	3.4867	3.4860	3.4868	3.4912	3.4908
⁴⁸ Ca	3.4771	3.4935	3.4890	3.4889	3.494	3.4890	3.4895	3.4891	3.4935	3.4906	3.4916	3.5023	3.5020
⁵⁰ Ca	3.5168	3.5157		3.5122	3.515	3.5130		3.5077	3.5155		3.5112		3.5180
⁵⁰ Ti	3.5704	3.5537	3.5558	3.5543	3.555	3.5522	3.5696	3.5673	3.5680	3.5664	3.5648	3.5868	3.5846
⁵⁸ Ni	3.7757	3.7358	3.7372	3.7362	3.737	3.7308	3.7761	3.7744	3.7621	3.7645	3.7652	3.8065	3.8055
⁶⁰ Ni	3.8118	3.7676		3.7673	3.768	3.7637		3.7972	3.7865		3.7892		3.8246
⁶² Ni	3.8399	3.7983		3.7982	3.797	3.7961		3.8211	3.8136		3.8135		3.8445
⁶⁴ Ni	3.8572	3.8275		3.8278	3.827	3.8270		3.8449	3.8408		3.8372		3.8644
⁸⁶ Kr	4.1835	4.1818		4.1813	4.180	4.1801		4.1823	4.1847		4.1821		4.1965
⁸⁸ Sr	4.2240	4.2245	4.2247	4.2240	4.223	4.2222	4.2231	4.2218	4.2250	4.2269	4.2261	4.2379	4.2365
⁹⁰ Zr	4.2694	4.2688	4.2695	4.2681	4.267	4.2662	4.2664	4.2654	4.2673	4.2724	4.2719	4.2847	4.2828
⁹² Mo	4.3151	4.3111	4.3125	4.3107	4.310	4.3081	4.3140	4.3120	4.3112	4.3192	4.3178	4.3333	4.3308
¹⁰⁸ Sn	4.5605	4.5455		4.5456	4.544	4.5417		4.5572	4.5486		4.5562		4.5774
¹¹⁰ Sn	4.5785	4.5645		4.5647	4.563	4.5613		4.5738	4.5673		4.5728		4.5922
¹¹² Sn	4.5948	4.5825	4.5801	4.5826	4.582	4.5796	4.5894	4.5891	4.5849	4.5870	4.5883	4.6044	4.6059
¹¹⁴ Sn	4.6099	4.5993		4.5993	4.599	4.5967		4.6030	4.6014		4.6028		4.6186
¹¹⁶ Sn	4.6250	4.6150	4.6121	4.6148	4.614	4.6126	4.6174	4.6165	4.6168	4.6168	4.6164	4.6307	4.6314
¹¹⁸ Sn	4.6393	4.6299		4.6293	4.629	4.6275		4.6300	4.6314		4.6296		4.6447
¹²⁰ Sn	4.6519	4.6441		4.6431	4.643	4.6417		4.6435	4.6455		4.6424		4.6582
¹²² Sn	4.6634	4.6579	4.6561	4.6566	4.657	4.6553	4.6579	4.6571	4.6593	4.6549	4.6552	4.6728	4.6718
¹²⁴ Sn	4.6735	4.6714	4.6694	4.6698	4.670	4.6687	4.6714	4.6708	4.6727	4.6677	4.6681	4.6864	4.6856
¹²⁶ Sn	4.6833	4.6847		4.6830	4.683	4.6819		4.6844	4.6859		4.6812		4.6994
¹²⁸ Sn	4.6921	4.6979		4.6961	4.696	4.6949		4.6981	4.6987		4.6943		4.7134
¹³⁰ Sn	4.7019	4.7108		4.7091	4.709	4.7078		4.7116	4.7111		4.7074		4.7274
¹³² Sn	4.7093	4.7232		4.7218	4.722	4.7205		4.7250	4.7229		4.7202		4.7415
¹³⁴ Te	4.7569	4.7691		4.7682	4.767	4.7666		4.7693	4.7683		4.7663		4.7850
¹³⁶ Xe	4.7964	4.8116		4.8107	4.809	4.8089		4.8108	4.8104		4.8088		4.8261
¹³⁸ Ba	4.8378	4.8513	4.8508	4.8503	4.848	4.8483	4.8511	4.8501	4.8497	4.8494	4.8487	4.8667	4.8654
¹⁴⁰ Ce	4.8771	4.8883	4.8879	4.8872	4.885	4.8850	4.8879	4.8867	4.8861	4.8871	4.8861	4.9037	4.9024
¹⁴² Nd	4.9123	4.9217		4.9209	4.919	4.9183		4.9188	4.9199		4.9204		4.9337
¹⁴⁴ Sm	4.9524	4.9541	4.9544	4.9534	4.951	4.9504	4.9521	4.9505	4.9523	4.9547	4.9539	4.9676	4.9657
¹⁴⁶ Gd	4.9801	4.9862		4.9857	4.983	4.9822		4.9829	4.9846		4.9875		4.9989
¹⁴⁸ Dy	5.0455	5.0183		5.0179	5.015	5.0139		5.0161	5.0169		5.0212		5.0328
¹⁵⁰ Er	5.0548	5.0501		5.0499	5.047	5.0454		5.0493	5.0490		5.0546		5.0666
²⁰⁶ Hg	5.4837	5.5053		5.5036	5.503	5.5006		5.4967	5.4949		5.4995		5.5121
¹⁸² Pb	5.3788	5.3856		5.3846	5.384	5.3793		5.3813	5.3811		5.3877		5.3955
¹⁸⁴ Pb	5.3930	5.3966		5.3952	5.394	5.3900		5.3916	5.3919		5.3977		5.4056
¹⁸⁶ Pb	5.4027	5.4076		5.4059	5.405	5.4008		5.4023	5.4028		5.4080		5.4160
¹⁸⁸ Pb	5.4139	5.4185		5.4167	5.416	5.4116		5.4131	5.4136		5.4183		5.4267
¹⁹⁰ Pb	5.4222	5.4295		5.4275	5.427	5.4225		5.4239	5.4243		5.4287		5.4375
¹⁹² Pb	5.4300	5.4403		5.4383	5.438	5.4334		5.4347	5.4349		5.4390		5.4484
¹⁹⁴ Pb	5.4372	5.4511		5.4490	5.448	5.4443		5.4454	5.4453		5.4493		5.4593
¹⁹⁶ Pb	5.4444	5.4618		5.4596	5.459	5.4550		5.4560	5.4556		5.4595		5.4702
¹⁹⁸ Pb	5.4524	5.4723		5.4701	5.470	5.4657		5.4664	5.4656		5.4696		5.4808
²⁰⁰ Pb	5.4611	5.4826		5.4804	5.480	5.4762		5.4766	5.4754		5.4796		5.4913
²⁰² Pb	5.4705	5.4928	5.4908	5.4905	5.490	5.4865	5.4869	5.4865	5.4849	5.4892	5.4893	5.4996	5.5014
²⁰⁴ Pb	5.4803	5.5026	5.5005	5.5003	5.500	5.4966	5.4962	5.4960	5.4940	5.4987	5.4988	5.5112	5.5110
²⁰⁶ Pb	5.4902	5.5119	5.5098	5.5098	5.509	5.5063	5.5049	5.5047	5.5027	5.5078	5.5079	5.5200	5.5197
²⁰⁸ Pb	5.5012	5.5204	5.5185	5.5186	5.518	5.5154	5.5129	5.5128	5.5109	5.5162	5.5162	5.5279	5.5275
²¹⁰ Pb	5.5208	5.5405		5.5385	5.538	5.5346		5.5327	5.5292		5.5363		5.5464
²¹² Pb	5.5396	5.5599		5.5580	5.558	5.5539		5.5520	5.5472		5.5556		5.5649
²¹⁴ Pb	5.5577	5.5789	5.5798	5.5773	5.578	5.5730	5.5711	5.5707	5.5650	5.5762	5.5743	5.5813	5.5828
²¹⁰ Po	5.5704	5.5554		5.5540	5.552	5.5346		5.5468	5.5459		5.5513		5.5606
²¹² Rn	5.5915	5.5884		5.5871	5.585	5.5836		5.5792	5.5791		5.5840		5.5922
²¹⁴ Ra	5.6079	5.6200		5.6188	5.617	5.6151		5.6103	5.6108		5.6153		5.6229
rms ₂₃ ^a		0.0224	0.0222	0.0220	0.0217	0.0222	0.0197	0.0197	0.0195	0.0197	0.0194	0.0250	0.0247
rms ₆₃ ^a		0.0187		0.0183	0.0182	0.0187		0.0157	0.0153		0.0153		0.0211
rrs ₂₃		0.68%	0.68%	0.67%	0.67%	0.69%	0.58%	0.59%	0.61%	0.61%	0.61%	0.67%	0.66%
rrs ₆₃		0.51%		0.50%	0.50%	0.52%		0.44%	0.43%		0.43%		0.51%

The experimental data is quoted from the compilation by Angeli & Marinova [53]. See the footnote of Tables 2 and S3 for further description of the theoretical data.